mathematics

MDPI

Article

Neurodegenerative Disease-Specific Relations Between Temporal and Kinetic Gait Features Identified Using InterCriteria Analysis

Irena Jekova *, Vessela Krasteva and Todor Stoyanov

Institute of Biophysics and Biomedical Engineering, Bulgarian Academy of Sciences, Acad. G. Bonchev Str. Bl. 105, 1113 Sofia, Bulgaria; vessika@biomed.bas.bg (V.K.); todor@biomed.bas.bg (T.S.)
* Correspondence: irena@biomed.bas.bg

Abstract

Gait analysis is a non-invasive, cost-effective method for detecting subtle motor changes in neurodegenerative disorders. This study uses an exploratory approach to identify temporal–kinetic gait feature relationships specific to amyotrophic lateral sclerosis (ALS) and Huntington (HUNT) and Parkinson (PARK) disease versus healthy controls (CONTROL) using recent advances in InterCriteria Analysis (ICrA). The novelty lies in the (i) comprehensive temporal–kinetic feature set, (ii) use of ICrA to characterize inter-feature coordination patterns at population and disease-group levels and (iii) interpretation in a neuromechanical context. Forty-one temporal/kinetic features were extracted from left/right leg ground reaction force and rate-of-force-development signals, considering laterality, gait phase (stance, swing, double support), magnitudes, waveform correlations, and inter-/intra-limb asymmetries. The analysis included 14,580 steps from 64 recordings in the Gait in Neurodegenerative Disease Database: 16 CONTROL (4054 steps), 13 ALS (2465), 20 HUNT (4730), 15 PARK (3331). Sensitivity analysis identified strict consonance thresholds ($\mu \geq 0.75$, $\nu \leq 0.25$), selecting <5% strongest inter-feature relations from 820 feature pairs: population level (16 positive, 14 negative), group-level (15–25 positive, 9–14 negative). ICrA identified group-specific consonances—present in one group but absent in others—highlighting disease-related alterations in gait coordination: ALS (15/11 positive/negative, disrupted bilateral stride coordination, prolonged stance/double-support, decoupled stride/cadence, desynchronized force-generation patterns—reflecting compensatory adaptations to muscle weakness and instability), HUNT (11/7, severe temporal–kinetic breakdown consistent with gait instability—loss of bilateral coordination, reduced swing time, slowed force development), PARK (1/2, subtle localized disruptions—prolonged stance and double-support intervals, reduced force during weight transfer, overall coordination remained largely preserved). Benchmarking vs. Pearson correlation showed strong linear agreement ($R^2 = 0.847$, $p < 0.001$), confirming that ICrA captures dominant dependencies while moderating the correlation via uncertainty. These results demonstrate that ICrA provides a quantitative, interpretable framework for characterizing gait coordination patterns and can guide principled feature selection in future predictive modeling.

Keywords: intuitionistic fuzzy sets; index matrices; consonance; dissonance; Parkinson; Huntington; amyotrophic lateral sclerosis (ALS); gait analysis; ground-reaction-force; rate of force development

MSC: 03E72; 03F55; 62P10; 92C50

Check for updates

Academic Editors: Stoyan Tranev and Velichka Traneva

Received: 10 December 2025
Revised: 13 January 2026
Accepted: 16 January 2026
Published: 19 January 2026

Copyright: © 2026 by the authors. Licensee MDPI, Basel, Switzerland. This article is an open access article distributed under the terms and conditions of the Creative Commons Attribution (CC BY) license.

1. Introduction

Neurodegenerative diseases (NDDs), due to cellular dysfunction or cell death at different brain regions, are one of the main causes of disability and mortality worldwide [1]. Common NDDs that have emerged as a significant concern in recent years due to their rising incidence include Parkinson's disease (PARK), Huntington's disease (HUNT), and amyotrophic lateral sclerosis (ALS) [2–4].

Parkinson's disease is commonly associated with the progressive degeneration of dopamine-producing neurons, which play an essential role in regulating and coordinating precise muscle movements [5–7]. It presents with non-motor symptoms such as sleep disturbances, constipation, depression, and anosmia, along with a range of movement-related complications. These include tremor, rigidity, and slow movements (bradykinesia), which contribute to reduced gait speed and shorter stride length. Gait abnormalities may also involve increased cadence, shuffling steps with insufficient foot clearance, episodic inability of feet movement (known as gait freezing), and a tendency to take rapid, short, involuntary steps either forward (festination) or backward (retropulsion) [8–12]. PARK affects approximately 0.3% of the general population and 1–3% of individuals over 65 years of age, with a global prevalence exceeding 8.5 million cases and continuing to rise [1,5].

Huntington's disease is caused by a genetic mutation in the huntingtin gene which results in the production of an abnormal form of the huntingtin protein [5,7]. It is associated with depression, irritability, and apathy, which often precede the physical symptoms. These motor manifestations include uncontrolled and uncoordinated body movements, such as lateral swaying and spontaneous knee flexion, an unsteady gait marked by alternating hyperkinesia and hypokinesia, reduced gait velocity, stride length, and cadence, and an increased stance phase [7,13,14]. Although rarer than PARK (reported prevalence $\approx$ 5–14 per 100,000), HUNT carries substantial morbidity and mortality, with the prevalence varying across populations due to genetic factors [1,5].

Amyotrophic lateral sclerosis is a motor neuron disease characterized by the progressive degeneration of nerve cells in the brain and spinal cord, leading to the loss of motor neurons responsible for controlling voluntary muscle contractions [5,7]. The symptoms initially include muscle weakness and difficulties with speech and swallowing, which may progress to paralysis and respiratory failure in the later stages of the disease. Gait is also affected, showing greater variability compared to healthy subjects, especially for stance and swing times, along with reduced a gait velocity, cadence, and stride length [15–17]. Patients spent less time in single-leg support and more time in double-support during walking. The reduced stride length is attributed to decreased hip excursion in the flexion and extension, excessive knee flexion at initial contact, and diminished plantarflexion during push-off [17]. ALS is a rare but highly lethal neurodegenerative disease ($\approx$1.9–6 per 100,000 globally) with a typical survival of only 2–5 years after diagnosis and high mortality, most often due to respiratory failure [1,5,18].

Beyond their clinical burden, these disorders impose substantial societal and economic costs that increase with disease progression. Reported per-patient annual costs range from several thousand euros to well over €100,000, depending on the disease stage, healthcare system, and indirect costs, with national expenditures reaching hundreds of millions to billions of euros annually across Europe and the United States [18–21].

The most important and commonly used biomarkers for diagnosing PARK and HUNT disease include magnetic resonance imaging (MRI), positron emission tomography (PET), single-photon emission computed tomography (SPECT), cerebrospinal fluid (CSF) analysis, and blood tests [7]. ALS diagnosis is primarily based on assessments of muscle strength, including maximal voluntary isometric contraction (MVIC) and the hand-held dynamometry test (HHDT), along with CSF analysis [7]. While MRI, PET, SPECT, CSF analyses, and

MVIC provide valuable information, they are often costly and time-consuming and require specialized expertise. Cheaper alternatives, such as the HHDT test have limited sensitivity to subtle or early changes [22,23]. In contrast, gait disturbances frequently emerge early in disease progression and evolve systematically as neurodegeneration advances [2,24–27].

Over the past decade, a novel mathematical technique called InterCriteria Analysis (ICrA) was developed to identify and quantify the levels of pairwise dependencies within a dataset [28]. The method has been further refined and enhanced to improve its accuracy and applicability across diverse fields [29–35]. The core concept of ICrA is to identify pairs of criteria that exhibit strong positive or negative consonance, thereby aiding in the selection of a meaningful set of criteria for decision-making processes. In recent years, ICrA has gained increasing attention for the optimization of various decision-making tasks in biomedicine and physiological data analysis. It has been applied to evaluate scoring functions in molecular modeling software [36], assess indicators associated with the health-related quality of life [37], and study interdependencies in diverse clinical datasets, including those from patients with colorectal cancer [38], myeloma [39], melanoma [40], Behterev's disease [41], cardiac arrhythmias [42], and menopausal genitourinary syndrome [43]. Additionally, ICrA has been effectively employed to analyze criteria derived from electromyographic (EMG) data, providing valuable insights into neuromuscular functions and optimizing experimental protocols. Specifically, it has been used to estimate the surface EMG activity of upper arm muscles [44], optimize experimental protocols for EMG signal measurements [45], assess the effects of transcranial magnetic stimulation intensities and muscle conditions on evoked responses of the first dorsal interosseous muscle [46], and evaluate the effects of movement speed and load on upper arm muscles in the horizontal plane [47].

Building on these advances, the present study aims to explore the potential of ICrA to identify the relational structure of the gait in specific neurodegenerative disorders. By capturing interdependencies among multiple temporal and kinetic gait features—relationships that are not accessible through conventional single-feature analyses—this approach contributes to gait analysis as an emerging diagnostic modality that is non-invasive, inexpensive, and increasingly recognized for its ability to detect subtle motor alterations that may appear years before clinical symptoms become evident.

To provide a comprehensive overview of gait organization, the first part of the study constructs a high-dimensional dataset comprising more than 40 temporal and kinetic gait features derived from ground reaction force and rate-of-force-development signals collected from healthy individuals and patients with ALS, Huntington's disease, and Parkinson's disease. In the second analytical phase, rather than developing or validating a new diagnostic model, ICrA is employed to examine how multiple gait features co-vary and form coordination patterns that distinguish a healthy from pathological gait. Specifically, intercriteria relationships are analyzed within and across the four groups to identify group-specific consonances—relational patterns present in one group but absent in others. These patterns highlight structural alterations in gait organization associated with each disorder, provide insight into disease-specific neuromechanical dysfunction, and may inform future feature-selection strategies for machine-learning pipelines.

2. Materials and Methods

2.1. Database

The present study used data from the Gait in Neurodegenerative Disease Database (GNDD, Version 1.0.0) [16,48,49], publicly available via the PhysioNet archive. The database contains 64 gait recordings, including 16 healthy controls (CONTROL) and 48 patients distributed across three NDD groups: 20 with HUNT, 15 with PARK, and 13 with ALS. Data were fully anonymized prior to public release, and only non-identifiable subject

codes are available to third-party users. The GNDD data were collected under institutional ethics committee approval. Secondary research use of the dataset is authorized under the PhysioNet data-sharing agreement.

Raw gait data were acquired using force-sensitive resistors placed under each foot, with the sensor output approximately proportional to the ground reaction force (GRF). Each subject's dataset comprises four files: two binary files (.let, .rit) containing synchronous left- and right-foot ground force signals recorded over approximately 300 s of walking, a header file (.hea), and a derived time-series file (.ts) that includes pre-computed gait-cycle features calculated for each step, as detailed in the following section. The initial 20 s of each GRF recording was discarded to skip the initialization process, which normally does not contain the normal walk pattern and valid gait-cycle features. Across the dataset, the number of available steps per recording ranged from 122 to 310, with a mean of 237 $\pm$ 35 steps. The distribution of step counts within the four subject groups, together with the demo-graphic characteristics, is summarized in Table 1.

Table 1. Demographic characteristics of the subjects included in the Gait in Neurodegenerative Disease Database (Version 1.0.0) [49], divided into four groups—CONTROL: Healthy controls, ALS: amyotrophic lateral sclerosis, HUNT: Huntington's disease, PARK: Parkinson's disease. The last column reports the number of steps per recording for which temporal gait features are available in the corresponding time-series file (.ts). Continuous variables are presented as the mean value $\pm$ standard deviation.

Disease	Nb Subjects	Age (Years)	Height (m)	Weight (kg)	Gender	Steps
CONTROL	16	39 $\pm$ 19	1.83 $\pm$ 0.08	67 $\pm$ 11	12.5% male	255 $\pm$ 18
ALS	13	56 $\pm$ 13	1.74 $\pm$ 0.10	77 $\pm$ 21	76.9% male	196 $\pm$ 38
HUNT	20	47 $\pm$ 13	1.83 $\pm$ 0.11	72 $\pm$ 17	30% male	242 $\pm$ 30
PARK	15	67 $\pm$ 11	1.87 $\pm$ 0.15	75 $\pm$ 17	66.7% male	246 $\pm$ 24

2.2. Gait Features

The gait-related features examined in this study can be split in two main categories: 16 temporal features (identifier C1–C16) and 25 kinetic features (C17–C41). They are further explained in detail.

2.2.1. Temporal Gait Features

The brief description of 16 temporal features is summarized in Table 2, including the following:

- C01–C12: Twelve primary stride-to-stride temporal gait measures read directly from the database time-series (.ts) files. They characterize the stride interval, swing interval, stance interval, and double-support interval, provided both in the absolute time (seconds) and as a percentage of the stride for the left and right legs. Figure 1 (top) illustrates the sequence of intervals for the two legs in a normal gait. These fundamental temporal parameters follow established gait-analysis conventions and definitions [50–52] and are widely used to evaluate walking patterns, postural stability, and deviations from normative gait behavior [53–55].
- C13–C16: Four secondary temporal features capturing broader aspects of gait dynamics, including the cadence (walking rate), swing asymmetry (left–right imbalance in swing duration), swing variability (stride-to-stride fluctuations in swing timing), and gait variability (stride-interval instability reflecting reduced rhythmicity). All four measures are analytically derived from the primary temporal parameters (C01-C12) using the definitions summarized in Table 2. These descriptors are established markers of gait stability and motor impairment in NDD [51,56,57].

Table 2. Temporal gait features used in this study.

ID	Abbreviation	Description
Primary temporal features of the gait cycle		
C01	*LStrInt (s)*	Left stride interval: Time between two consecutive heel strikes of the left foot
C02	*RStrInt (s)*	Right stride interval: Time between two consecutive heel strikes of the right foot
C03	*LSwInt (s)*	Left swing interval: Duration when the left foot is not in contact with the ground during a stride
C04	*RSwInt (s)*	Right swing interval: Duration when the right foot is not in contact with the ground during a stride
C05	*LSwInt (% stride)*	Left swing interval expressed as a percentage of the left stride duration
C06	*RSwInt (% stride)*	Right swing interval expressed as a percentage of the right stride duration
C07	*LStanInt (s)*	Left stance interval: Time during which the left foot is in contact with the ground within a stride
C08	*RStanInt (s)*	Right stance interval: Time during which the right foot is in contact with the ground within a stride
C09	*LStanInt (% stride)*	Left stance interval expressed as a percentage of the left stride duration
C10	*RStanInt (% stride)*	Right stance interval expressed as a percentage of the right stride duration
C11	*DSupInt (s)*	Double-support interval: Total time within a stride when both feet are simultaneously in contact with the ground
C12	*DSupInt (% stride)*	Double-support interval expressed as a percentage of stride duration
Secondary temporal features of the gait dynamics		
C13	*Cadance (steps/minute)*	Number of steps taken per minute (walking rate).
C14	*SwAsymetry (% stride)*	Swing asymmetry: Difference between the left and right swing intervals, expressed as a percentage of the stride: $SwAssymetry\ (\%) = \lvert LSwInt\ (\%) - RSwInt\ (\%) \rvert$
C15	*SwVariability (%)*	Swing Variability: Stride-to-stride variability of the swing interval, quantifying how much the swing duration changes from one stride to the next. The formula is shown for the left leg, where n and n−1 denote the current and previous strides, respectively: $SwVariability_{(n)}(\%) = \left\lvert LSwInt_{(n)}(\%) - LSwInt_{(n-1)}(\%) \right\rvert$
C16	*GaitVariability (%)*	Gait variability: Stride-to-stride variability of the stride interval (in seconds), normalized by the duration of the current stride. The formula is expressed for the left leg, where n and n−1 denote the current and previous strides, respectively: $GaitVariability_{(n)}(\%) = \frac{\lvert LStrInt_{(n)}(s) - LStrInt_{(n-1)}(s) \rvert}{LStrInt_{(n)}(seconds)} \times 100$

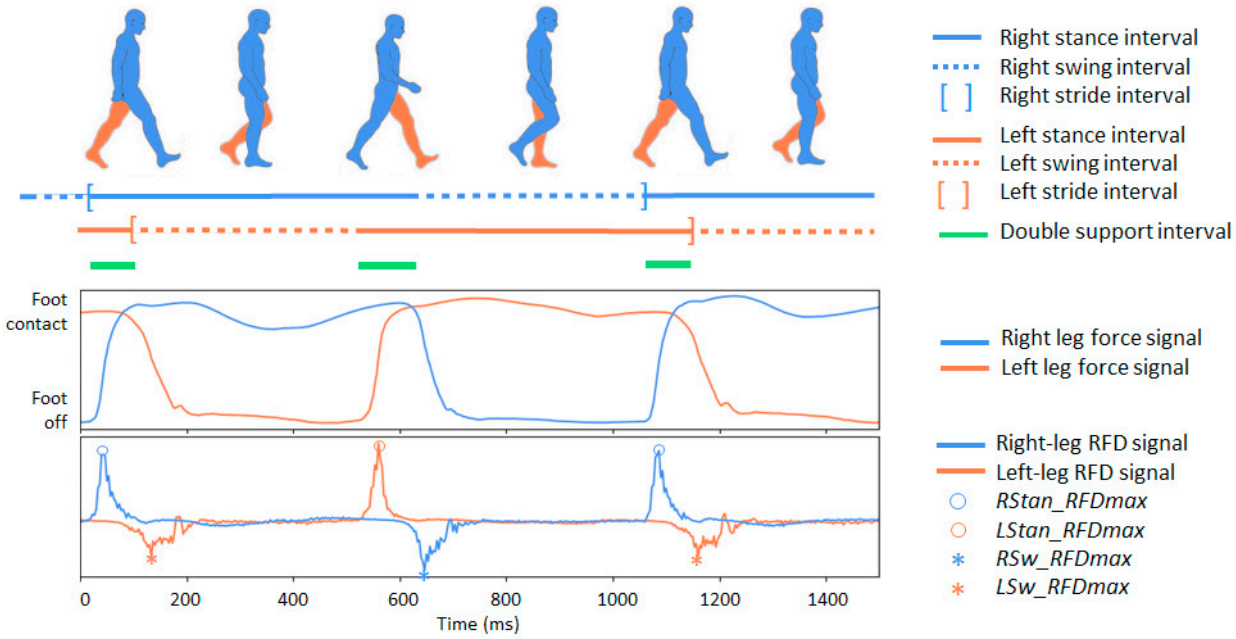


Figure 1. Illustration of the main phases of the human gait cycle. On top: the temporal progression of stance and swing phases for both legs during walking is depicted with separate lines, with the subsequent segment representing the double-support interval. In a normal gait, the stance phase (foot in contact with the ground) represents approximately 60% of the cycle, while the swing phase (foot in the air) represents about 40%. The double support interval (the brief period when both feet are simultaneously in contact with the ground) occurs twice within each gait cycle, once during the transition from left to right stance and once during the reverse transition. On the bottom: two signal traces that can be captured using a foot sensor during human gait: (1) ground reaction force signals for the right and left legs, as provided in the Gait in Neurodegenerative Disease Database; (2) calculated force-derivative denoted as the rate of force development (RFD), for both legs. Four kinetic RFD features are highlighted: the maximum positive RFD deflections during stance for the right and left foot (*RStan_RFDmax* and *LStan_RFDmax*), and the maximum negative RFD deflections during swing for the right and left foot (*RSw_RFDmax* and *LSw_RFDmax*).

2.2.2. Kinetic Gait Features

Twenty-five kinetic gait features are calculated from the raw ground reaction force (GRF) signals of the left and right foot and from the time derivative of the force signal, commonly referred to as the rate of force development (RFD), or *yank*. RFD provides a quantitative description of how rapidly muscle force, GRF, or joint moment changes over a predefined time interval and is considered an important descriptor of neuromuscular function across sensorimotor systems [58]. The magnitude and temporal profile of RFD are particularly relevant during rapid or reflexive actions, such as tripping or postural perturbations. These reflexive, gait-related disturbances are of primary interest in our study, as they are characteristic of NDDs.

In this study, RFD was computed as the first-order difference of the GRF signal F across a single sampling interval $\Delta T = 1/fs$, with a native sampling frequency fs = 300 Hz:

$$\mathrm{RFD(i)} = \frac{\mathrm{Fn(i)} - \mathrm{Fn(i-1)}}{\Delta T}, \tag{1}$$

where i and $i - 1$ denote two consecutive samples of the normalized force signal Fn. The normalization was performed on a step-by-step basis using min–max scaling:

$$\mathrm{Fn(i)} = \frac{\mathrm{Fstep(i)} - \min(\mathrm{Fstep})}{\max(\mathrm{Fstep}) - \min(\mathrm{Fstep})}, \tag{2}$$

where Fstep contains all force samples within a single step. Step durations were taken directly from the time-series (*.ts) database files without applying additional step-detection methods.

The step-wise min–max normalization in (2) ensures the same range of the force signal for each step and, consequently, the same scale of the derived RFD measures, facilitating inter-step and inter-participant comparisons and reducing the influence of differences in force-sensor acquisition conditions. By normalizing each step independently, long-term drift in the force signal is mitigated, addressing potential calibration drift and eliminating the need for high-pass filtering. Steps with missing or saturated GRF data were excluded from the analysis, preventing artifacts due to sensor saturation or nonlinear response, as kinetic features cannot be reliably computed in these cases. This preprocessing removes information about the absolute force magnitude, but prioritizes the analysis of relative force modulation and waveform structure within the gait cycle. Normalized or shape-based RFD measures are widely applied in studies of neuromuscular control and the temporal characteristics of rapid force production, as they reduce confounding effects of body mass, sensor coupling, and scaling while preserving physiologically meaningful timing behavior [59–61].

Because numerical differentiation can amplify high-frequency noise, RFD computation was implemented only after segmentation and step-level normalization of the GRF signal. The GRF recordings were sampled at 300 Hz with low sensor noise, and the RFD-based features used in this study were calculated as phase-level averages or extrema rather than point-wise derivative estimates, which substantially limits noise propagation. This approach is consistent with prior biomechanical work where GRF-derived or normalized RFD measures are used to study neuromuscular control and timing behavior rather than absolute contractile force capacity [59–61]. Additional smoothing was avoided to preserve physiologically meaningful rapid-force transitions, particularly during weight acceptance and push-off.

The kinetic and RFD-based features defined in Table 3 are grounded in established biomechanical and neuromechanical concepts of ground-reaction-force analysis and rate-of-force development. For clarity, their formulas for computation are provided in Table 3 where needed. The following groups of features are considered:

- C17–C25: Primary RFD features quantifying peak and average amplitudes of the force derivative for each leg during stance and swing. These follow standard definitions used to characterize neuromuscular force-generation capacity and gait stability [51,62,63].
- C26–C29: Inter-limb correlation features capturing bilateral symmetry in the left- and right-leg GRF and RFD waveforms over a step. Classical zero-lag and lag-optimized cross-correlation measures are employed to quantify bilateral waveform synchrony, as commonly applied in gait coordination and signal-processing analyses [52,64,65]. Zero-lag correlations (C26–C27) reflect both the waveform shape similarity and temporal alignment at identical time instants. For lag-optimized correlations (C28–C29), only the maximum correlation magnitude observed within the step interval is retained. These measures therefore quantify waveform-shape synchrony independent of explicit timing offset as the associated lag values are not further analyzed.
- C30–C33: Inter-limb RFD asymmetry features describing differences between the left and right legs in maximum and average RFD amplitudes during stance and swing.
- C34–C37: Intra-limb stance–swing RFD asymmetry features reflecting differences between stance and swing phases in maximum and average RFD amplitudes within each leg.

- C38–C41: Global stance–swing RFD asymmetry features capturing the following: (i) differences between stance and swing in maximum and average RFD amplitudes averaged across both legs; and (ii) ratios of stance- and swing-phase RFD amplitudes relative to double-support.

The asymmetry descriptors C30–C41 expressed as normalized absolute differences or ratios, follow widely used gait symmetry and phase-modulation indices applied in both healthy and pathological gait studies [52,66–68].

Table 3. Kinetic gait features computed in this study from the raw ground-reaction-force (GRF) signals of the left and right food. RFD: rate of force development. NDD: neurodegenerative disorder.

ID	Abbreviation	Description
Primary RFD Features (Force-Derivative Based)		
C17	*LStan_RFDmax*	Maximum positive deflection of the left-leg RFD signal during the stance interval—illustrated in Figure 1 (bottom). Represents the peak rate at which force is generated by the left leg while in ground contact. This value reflects the leg's ability to rapidly produce force during weight acceptance and propulsion—critical components of a stable gait. Reduced or delayed stance-phase RFDmax is frequently observed in individuals with impaired neuromuscular control, such as those with NDDs.
C18	*LSw_RFDmax*	Maximum negative deflection of the left-leg RFD signal during the swing interval (absolute value used)—illustrated in Figure 1 (bottom). Captures the largest rate of force fluctuation while the left foot is off the ground. Although overall forces are lower during swing, RFDmax reflects rapid limb deceleration/acceleration needed for foot clearance and step preparation. Abnormalities may indicate impaired motor coordination or compensatory movement strategies.
C19	*RStan_RFDmax*	Maximum positive deflection of the right-leg RFD signal during the stance interval—illustrated in Figure 1 (bottom). Right-leg analogue of C17. Indicates the capacity of the right leg to rapidly generate force during ground contact. Asymmetry between C17 and C19 may highlight unilateral weakness, a gait imbalance, or NDD-specific lateralization.
C20	*RSw_RFDmax*	Maximum negative deflection of the right-leg RFD signal during the swing interval (absolute value used)—illustrated in Figure 1 (bottom). Right-leg analogue of C18. Reflects rapid force changes during the right leg's swing phase. Elevated variability or reduced peaks can indicate difficulties in limb control or instability during segmental transitions.
C21	*LStan_RFDavg*	Average of the absolute left-leg RFD signal during the stance interval. Represents the overall rate of force development sustained throughout the stance phase on the left side. Unlike C17 (which captures the peak), this feature describes the general force-generation profile. Lower average RFD may correspond to reduced push-off efficiency or diminished neuromuscular responsiveness.
C22	*LSw_RFDavg*	Average of the absolute left-leg RFD signal during the swing interval. Reflects the average rate at which force changes occur while the left foot is in the air. This measure indicates the smoothness of limb motion and the consistency of force regulation during swing, both of which may be impaired in NDD gait.
C23	*RStan_RFDavg*	Average of the absolute right-leg RFD signal during the stance interval. The right-leg analogue to C21, capturing the mean force-development rate while the leg supports body weight. Comparing C21 and C23 provides insight into stance-phase symmetry and inter-limb coordination.
C24	*RSw_RFDavg*	Average of the absolute right-leg RFD signal during the swing interval. Complementing C22, this metric characterizes the force-change dynamics of the right leg during swing. Altered values may indicate difficulties in executing controlled, rhythmic limb advancement.

Table 3. *Cont.*

ID	Abbreviation	Description
C25	*DSup_RFDavg*	Average of the absolute RFD signal during double support interval. Separate values are measured from the RFD for the left and right legs and averaged. This measure reflects how quickly force is generated jointly by both legs during one of the most stability-critical phases of gait. Double support requires smooth and coordinated load transfer from one limb to the other; thus, abnormalities in *DSup_RFDavg* may indicate compromised balance control or impaired bilateral coordination—frequent findings in NDD.
Inter-limb Synchrony Features (Force and RFD Correlation)		
C26	*CorLR_F(lag0)*	Zero-lag correlation between left and right raw force signals within a stride. This feature quantifies how synchronized both legs are in producing ground reaction forces at the same moment. High values indicate smooth bilateral coordination, whereas reduced synchrony may reflect impaired timing, asymmetry, or compensatory loading strategies commonly observed in NDD gait.
C27	*CorLR_RFD(lag0)*	Zero-lag correlation between left and right RFD signals within a stride. Captures how closely the instantaneous force-generation dynamics of both legs align in time. Because RFD reflects neuromuscular responsiveness, this metric is sensitive to disruptions in bilateral motor control and can highlight subtle coordination deficits.
C28	*CorLR_F(maxlag)*	Maximum cross-correlation between left- and right-leg force signals computed across the duration of a single step. This feature identifies the highest possible bilateral synchrony in the force waveform shape after allowing for any temporal shift between limbs within the step interval. A lower value indicates reduced coordination quality, even when optimally time-aligned.
C29	*CorLR_RFD(maxlag)*	Maximum cross-correlation between left- and right-leg RFD signals computed across the duration of a single step. This feature captures the highest similarity in neuromuscular force-generation dynamics between limbs when time-alignment is optimized within the step. Only the correlation magnitude is analyzed here; the lag at which it occurs is not interpreted further.
Left–Right Leg Asymmetry Features (%)		
C30	*Stan_RFDmax(L-R)%*	Percent asymmetry between legs in terms of maximum RFD deflection during the stance: $Stan_RFDmax(L-R)\% = \frac{\lvert LStan_RFDmax - RStan_RFDmax\rvert}{max(LStan_RFDmax, RStan_RFDmax)} \times 100$ Reflects unilateral differences in how force is rapidly produced during weight-bearing. Elevated asymmetry is often associated with unilateral weakness, impaired balance, or lateralized disease progression.
C31	*Sw_RFDmax(L-R)%*	Percent asymmetry between legs in terms of maximum RFD deflection during swing: $Sw_RFDmax(L-R)\% = \frac{\lvert LSw_RFDmax - RSw_RFDmax\rvert}{max(LSw_RFDmax, RSw_RFDmax)} \times 100$ Measures left–right differences in limb acceleration and control during swing. Larger values may indicate impaired motor coordination, reduced foot-clearance control, or abnormal limb sequencing.
C32	*Stan_RFDavg(L-R)%*	Percent asymmetry between legs in terms of average RFD during stance: $Stan_RFDavg(L-R)\% = \frac{\lvert LStan_RFDavg - RStan_RFDavg\rvert}{max(LStan_RFDavg, RStan_RFDavg)} \times 100$ Evaluates persistent loading imbalance rather than peak differences. Elevated asymmetry may signal chronic compensatory gait patterns.
C33	*Sw_RFDavg(L-R)%*	Percent asymmetry between legs in terms of average RFD during swing: $Sw_RFDavg(L-R)\% = \frac{\lvert LSw_RFDavg - RSw_RFDavg\rvert}{max(LSw_RFDavg, RSw_RFDavg)} \times 100$ Reflects sustained differences in inter-limb force-change dynamics during the non-contact portion of gait, often heightened in conditions with motor rhythm disruption.

Table 3. *Cont.*

ID	Abbreviation	Description
Intra-Limb Stance–Swing RFD Asymmetry (%)		
C34	*L_RFDmax(stance-swing)%*	Percent difference between left stance and left swing maximum RFD: $L_RFDmax(stance-swing)\% = \frac{\lvert LStan_RFDmax - LSw_RFDmax\rvert}{max(LStan_RFDmax, LSw_RFDmax)} \times 100$ Highlights how effectively the left leg adapts between load-bearing (stance) and limb-advancement (swing). Abnormal values may indicate poor phase modulation.
C35	*R_RFDmax(stance-swing)%*	Percent difference between right stance and right swing maximum RFD: $R_RFDmax(stance-swing)\% = \frac{\lvert RStan_RFDmax - RSw_RFDmax\rvert}{max(RStan_RFDmax, RSw_RFDmax)} \times 100$ Assesses intra-limb force-generation adaptability for the right leg. Phase-dependent modulation deficits are common in NDD gait patterns.
C36	*L_RFDavg(stance-swing)%*	Percent difference between left stance and left swing average RFD: $L_RFDavg(stance-swing)\% = \frac{\lvert LStan_RFDavg - LSw_RFDavg\rvert}{max(LStan_RFDavg, LSw_RFDavg)} \times 100$ Indicates whether the left leg maintains consistent force-change dynamics across phases. Reduced differentiation may reflect impaired gait rhythm or stiffened motor patterns.
C37	*R_RFDavg(stance-swing)%*	Percent difference between right stance and right swing average RFD: $R_RFDavg(stance-swing)\% = \frac{\lvert RStan_RFDavg - RSw_RFDavg\rvert}{max(RStan_RFDavg, RSw_RFDavg)} \times 100$ Provides the right-side analogue to C36, showing how the leg transitions between functional roles. Deviations often appear in asymmetric or progression-based gait impairments.
Global Stance–Swing RFD Asymmetry (%)		
C38	*RFDmax(stance-swing)%*	Percent difference between stance-phase and swing-phase maximum RFD, averaged across both legs: $RFDmax(stance) = (LStan_RFDmax + RStan_RFDmax)/2 RFDmax(swing) = (LSw_RFDmax + RSw_RFDmax)/2 RFDmax(stance-swing)\% = \frac{\lvert RFDmax(stance) - RFDmax(swing)\rvert}{max(RFDmax(stance), RFDmax(swing))} \times 100$ Reflects global phase-dependent differences in rapid force-generation capability. A healthy gait typically shows clear differentiation; reduced contrast may indicate impaired phase modulation or diminished neuromuscular flexibility.
C39	*RFDavg(stance-swing)%*	Percent difference between stance-phase and swing-phase average RFD, averaged across both legs: $RFDavg(stance) = (LStan_RFDavg + RStan_RFDavg)/2 RFDavg(swing) = (LSw_RFDavg + RSw_RFDavg)/2 RFDavg(stance-swing)\% = \frac{\lvert RFDavg(stance) - RFDavg(swing)\rvert}{max(RFDavg(stance), RFDavg(swing))} \times 100$ Quantifies the overall modulation of force-change dynamics between weight-bearing and limb-advancement phases. Altered values may signal global gait dysregulation, reduced adaptability, or impaired neuromechanical control.
C40	*DSup_to_Stan_RFD%*	Ratio between double-support RFD and stance-phase maximal RFD. This feature quantifies how the average bilateral rate of force development during the double-support interval compares with the maximum RFD observed during stance, averaged across both legs. It expresses how force-generation dynamics during double support relate to the peak force-generation capacity during single-leg loading: $DSup_to_Stan_RFD\% = \frac{DSup_RFDavg}{(LStan_RFDmax + RStan_RFDmax)/2} \times 100$
C41	*DSup_to_Sw_RFD%*	Ratio between double-support RFD and swing-phase maximal RFD. This feature quantifies how the average bilateral rate of force development during the double-support interval compares with the maximum RFD measured during the swing phase, averaged across both legs. It reflects how force-generation capability during double support relates to the peak force-production capacity when each leg is unloaded and preparing for the next stance phase: $DSup_to_Sw_RFD\% = \frac{DSup_RFDavg}{(LSw_RFDmax + RSw_RFDmax)/2} \times 100$

2.3. InterCriteria Analysis

ICrA [28] integrates two mathematical frameworks—index matrices (IMs) [69,70] and intuitionistic fuzzy sets (IFSs) [71–73], to identify positive consonance, negative consonance, or dissonance between features.

An IM, typically denoted as $[O, C, e_{o,c}]$, is defined as an object of the following form:

	C_1	...	C_k	...	C_n
O_1	e_{O_1,C_1}	...	e_{O_1,C_k}	...	e_{O_1,C_n}
...	...	...	...	...	...
O_i	e_{O_i,C_1}	...	e_{O_i,C_k}	...	e_{O_i,C_n}
...	...	...	...	...	...
O_m	e_{O_m,C_1}	...	e_{O_m,C_k}	...	e_{O_m,C_n}

In terms of ICrA, the set of rows $O = \{O_1, \ldots, O_m\}$ represents the evaluated objects, while the set of columns $C = \{C_1, \ldots, C_n\}$ stands for criteria that describe each object. The element e_{O_i,C_k} $(1 \leq i \leq m, 1 \leq k \leq n)$ is the value of the $k^{\text{-th}}$ criterion measured for the $i^{\text{-th}}$ object and is comparable according to relation R with all other elements of IM.

An intuitionistic fuzzy pair (IFP) is an ordered pair $\langle \mu, \nu \rangle$, where μ, ν [0, 1] and $\mu + \nu \leq 1$. As fundamental elements of the intuitionistic fuzzy logics and ICrA, the IFP components μ and ν are interpreted as the degrees of membership (validity, agreement, etc.) and non-membership (non-validity, disagreement, etc.), respectively.

The main idea of ICrA is to perform pairwise comparisons between every two distinct criteria across all evaluated objects, as illustrated in Figure 2. To this end, ICrA analyzes an IM of size $m \times n$, representing m objects characterized by n criteria, and produces an $n \times n$ table containing intuitionistic fuzzy pairs that quantify the intercriteria correlations. The full mathematical foundations of ICrA are provided in [28]. A brief overview is presented below.

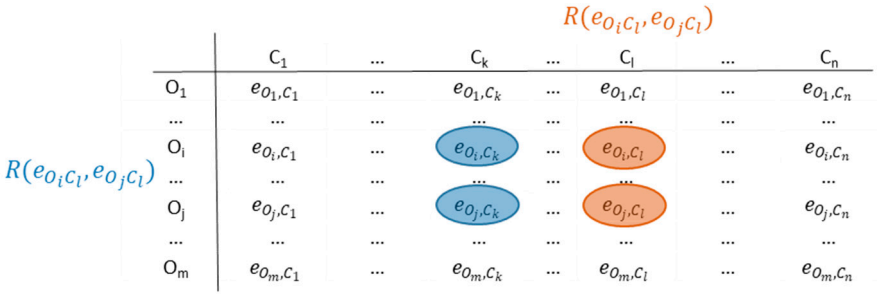


Figure 2. Intercriteria correlations.

The relation $R(e_{O_i,C_k}, e_{O_j,C_k})$ has a dual relation $\overline{R}$, which is true in the cases when R is false and vice versa. Two intuitionistic fuzzy counters, $S^{\mu}_{k,l}$ and $S^{\nu}_{k,l}$, are constructed and incremented according to the following rules:

- $S^{\mu}_{k,l}$ counts the number of cases in which the relations $R(e_{O_i,C_k}, e_{O_j,C_k})$ and $R(e_{O_i,C_l}, e_{O_j,C_l})$ (or their duals $\overline{R}(e_{O_i,C_k}, e_{O_j,C_k})$ and $\overline{R}(e_{O_i,C_l}, e_{O_j,C_l})$) are simultaneously satisfied.
- $S^{\nu}_{k,l}$ counts the number of cases in which $R(e_{O_i,C_k}, e_{O_j,C_k})$ and $\overline{R}(e_{O_i,C_l}, e_{O_j,C_l})$ (or $\overline{R}(e_{O_i,C_k}, e_{O_j,C_k})$ and $R(e_{O_i,C_l}, e_{O_j,C_l})$) are simultaneously satisfied.

Since the total number of pairwise comparisons between objects is $m(m-1)/2$, it follows that $0 \leq S^{\mu}_{k,l} + S^{\nu}_{k,l} \leq \frac{m(m-1)}{2}$. For each pair (k, l) with $1 \leq k \leq l \leq m$ and $m \geq 2$, two values are defined by normalizing $S^{\mu}_{k,l}$ and $S^{\nu}_{k,l}$ as follows:

- $\mu_{C_k,C_l} = 2\frac{S^{\mu}_{k,l}}{m(m-1)}$ which, in terms of ICrA, is known as the degree of agreement or positive consonance, and
- $\nu_{C_k,C_l} = 2\frac{S^{\nu}_{k,l}}{m(m-1)}$, known as degree of disagreement or negative consonance.

Both positive and negative consonances are numbers in the interval [0, 1], and their sum also remains in this range. The number that complements their sum ($\mu_{C_k,C_l} + \nu_{C_k,C_l}$) to 1 is denoted as π_{C_k,C_l}, representing the degree of uncertainty—a characteristic component of fuzzy and intuitionistic fuzzy methodologies [74–76]. Given that $\mu_{C_k,C_l} + \nu_{C_k,C_l} + \pi_{C_k,C_l} = 1$, any two of these three quantities are sufficient to characterize the degrees of agreement, disagreement, and uncertainty between two criteria.

Finally, the ICrA output consists of the calculated IFPs $\langle \mu_{C_k,C_l}, \nu_{C_k,C_l} \rangle$ that characterize the relationship between any two criteria C_k and C_l, defined in the input IM:

		C_1	...	C_k	...	C_n
C_1		$\langle 1,0 \rangle$	...	$\langle \mu_{C_1,C_k}, \nu_{C_1,C_k} \rangle$	...	$\langle \mu_{C_1,C_n}, \nu_{C_1,C_n} \rangle$
...		...	...	...	...	...
C_k		$\langle \mu_{C_k,C_1}, \nu_{C_k,C_1} \rangle$	...	$\langle 1,0 \rangle$	...	$\langle \mu_{C_k,C_n}, \nu_{C_k,C_n} \rangle$
...		...	...	...	...	...
	C_n	$\langle \mu_{C_n,C_1}, \nu_{C_n,C_1} \rangle$	...	$\langle \mu_{C_n,C_k}, \nu_{C_n,C_k} \rangle$	...	$\langle 1,0 \rangle$

From a practical standpoint, it is more convenient to work with the two separate index matrices IM_{μ} and IM_{ν}, rather than with the combined index matrix of IF pairs presented above.

The output of ICrA provides an estimation of the intercriteria relations as $\langle \mu, \nu \rangle$ pairs, which are typically presented in a square matrix of the format shown in Figure 3 (left). Based on user selected thresholds $\alpha, \beta \in [0, 1]$ for μ_{C_k,C_l} and ν_{C_k,C_l}, respectively, the relationship between any two criteria C_k and C_l is classified as follows:

- positive consonance, if $\mu_{C_k,C_l} > \alpha$ and $\nu_{C_k,C_l} < \beta$;
- negative consonance, if $\mu_{C_k,C_l} < \beta$ and $\nu_{C_k,C_l} > \alpha$;
- dissonance, otherwise.

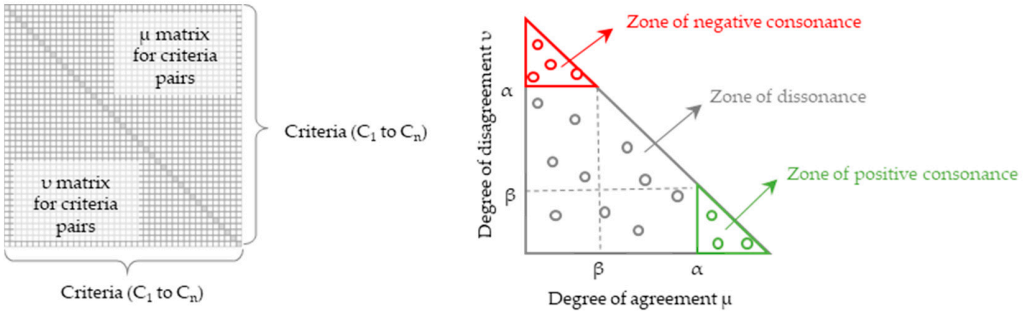


Figure 3. Typical presentation of the results from InterCriteria Analysis. On the left: output $\langle \mu, \nu \rangle$ matrix showing the relationships among criteria C_1 to C_n. For each of the $n(n-1)/2$ criterion pairs, the degree of agreement (μ) and the degree of disagreement (ν) are displayed above and below the main diagonal, respectively. On the right: intuitionistic fuzzy triangle plotted with μ on the x-axis and ν on the y-axis. The diagram highlights three regions separated by the α and β thresholds: the bottom-right zone of positive consonance (green), the upper-left zone of negative consonance (red), and the middle zone of dissonance (gray). Circles indicate the individual $\langle \mu, \nu \rangle$ values calculated for the different criterion pairs, which may fall within any of these regions.

For an illustration of the ICrA results, the well-known intuitionistic fuzzy interpretation triangle is used (Figure 3, right) [72]. It visualizes the thresholds α and β, along with the corresponding regions of positive consonance, negative consonance, and dissonance. The conventions for threshold selection within the ICrA framework are described in Atanassova et al. (2014) [77] and Doukovska et al. (2019) [31]. These authors emphasize that the thresholds are not fixed universal constants, but should instead be selected so as to balance theoretical interpretability with practical usefulness, allowing the decision-maker to regulate how many criterion pairs are ultimately regarded as positively or negatively consonant.

In this study, we adopted a predefined selection criterion whereby up to 5% of all criterion pairs should be classified as strongly consonant. This user-defined limit was chosen to ensure that only the most prominent and consistent relationships among gait features were retained for interpretation, while avoiding inflation through the inclusion of numerous weak or spurious associations. To identify which α/β consonance thresholds satisfied this condition, we performed a sensitivity analysis in which the proportion of criterion pairs classified as consonant was computed for α ranging from 1.0 to 0.0 (with $\beta = 1 - \alpha$). The final threshold was defined as the highest α value for which no more than 5% of all criterion pairs were classified as strongly consonant.

It should be noted that the ICrA methodology is inherently scale-invariant. Pairwise comparisons between criteria are based on relative agreement or disagreement, quantified through $\langle \mu, \nu \rangle$ pairs, rather than the absolute magnitudes of feature values. Consequently, the normalization or standardization of individual features is not required, as the computation of positive and negative consonances preserves the internal structure of each criterion. This scale-invariant property has been consistently applied in prior biomedical and physiological studies without the need for feature scaling [28–47].

3. Results

3.1. Test Setting

An overview of the complete data-processing and analysis pipeline is provided in Figure 4. The data from the GNDD database were accessed using the freely distributable Waveform Database (WFDB) software package for Python (version 4.1.2) [48,78]. This standardized PhysioNet toolkit supports the reliable reading, writing, and processing of physiological signals and annotations, ensuring correct handling of the input data format. Temporal and kinetic gait features were computed in Python (version 3.9) using the packages NumPy (1.23), pandas (1.5), and Matplotlib (3.10), following the procedures described in Sections 2.2.1 and 2.2.2 and the formulas listed in Tables 2 and 3. Using the available data for all steps and ground force signals without data loss, we computed 41 human gait features for a total of 14,580 steps (CONTROL: 4054; ALS: 2465; HUNT: 4730; PARK: 3331).

The computed feature values were stored in a CSV table and subsequently imported into the standalone ICrAData application for Windows (version 2.3; https://intercriteria.net/software/icradata/ (accessed on 6 January 2026)), described in detail in [79], to apply the ICrA methodology and examine relationships among gait features. The ICrA procedure was applied exactly as implemented in the ICrAData software, without any modification of the underlying theory, algorithm, or parameterization. ICrA was performed using the following configuration: ICrA Method = "Standard" and ICrA Variant = "μ-based".

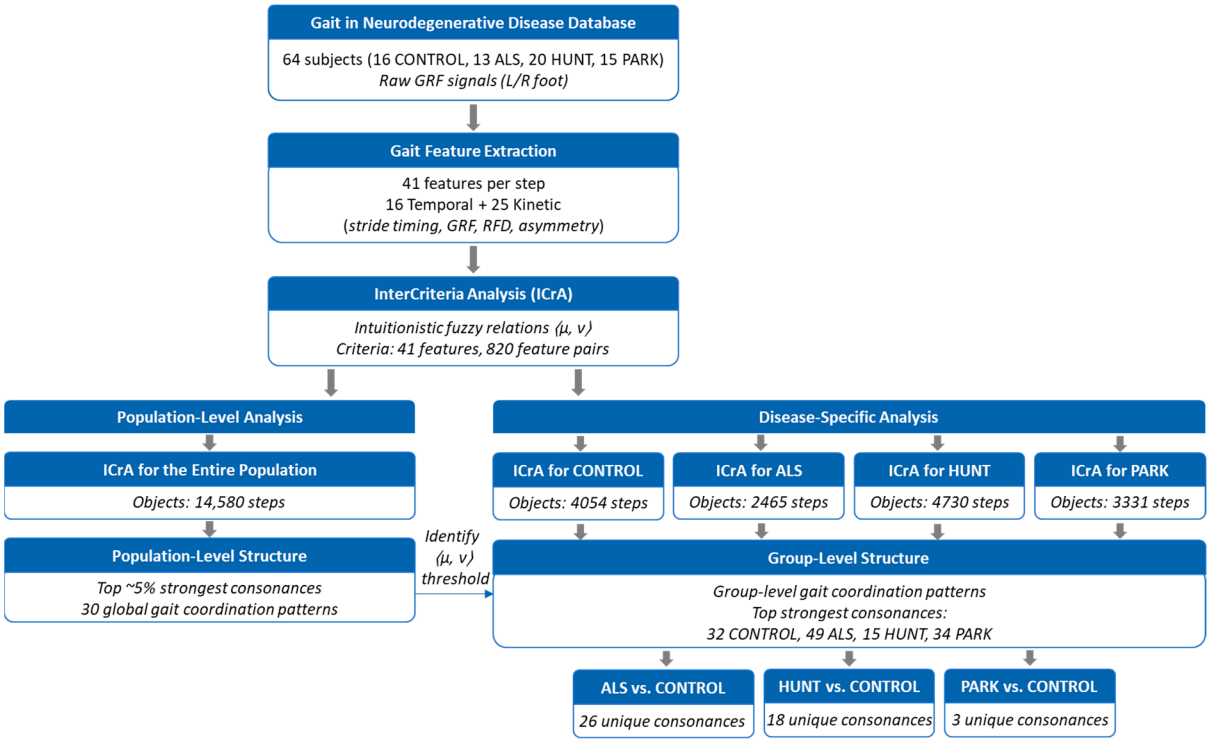


Figure 4. Overview of the analytical workflow. CONTROL: healthy controls, ALS: amyotrophic lateral sclerosis patients, HUNT: Huntington's disease patients, PARK: Parkinson's disease patients; GRF: ground reaction force; RFD: Rate of force development.

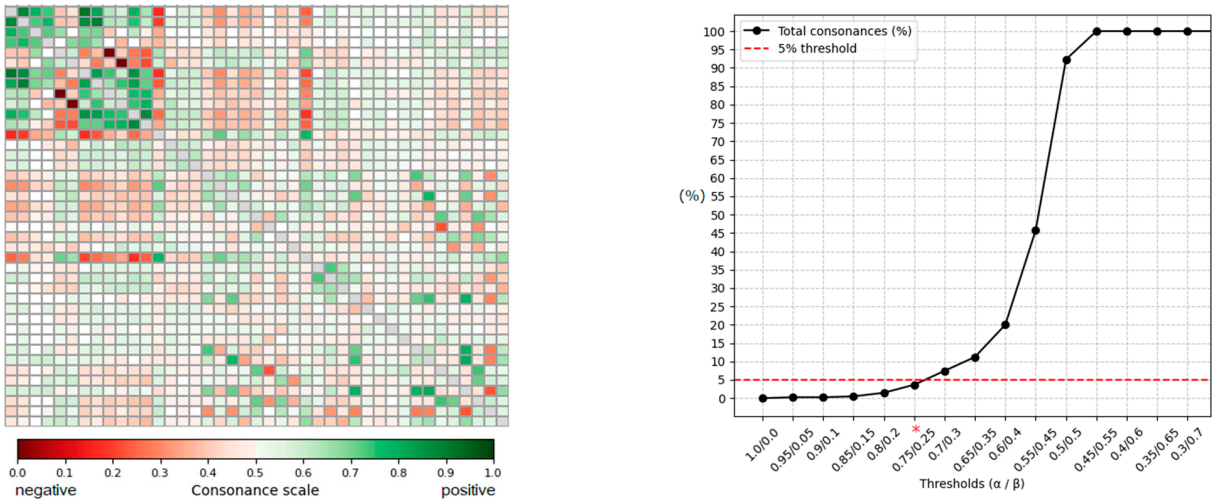
To evaluate computational scalability, we measured the runtime of the ICrA analysis for datasets of different sizes. Each step is represented by 41 gait features, yielding 820 unique feature–pair relations per step. For the full dataset (14,580 steps; 11.96 million feature-pair relations), the ICrAData software required 115 s on a workstation equipped with an Intel® Xeon® E5-2630 CPU @ 2.30 GHz (two processors), 32 GB RAM, Windows 10—corresponding to ~104,000 feature-pair evaluations per second. Group-level datasets required 9 s (CONTROL: 4054 steps), 6 s (PARK: 3331 steps), and 3 s (ALS: 2465 steps). Since the number of features is fixed, runtime scales approximately linearly with the number of steps, demonstrating that the workflow is computationally efficient and suitable for substantially larger gait databases. In addition, we measured the computation time for extracting all 41 gait features per step in Python. Using 100 randomly selected steps, the mean per-step computation time was 0.012 s $\pm$ 0.0068 s, confirming that feature extraction is fast and scales linearly with the number of steps.

Further the results of the study were considered in two analytical contexts:

1. Population-level intercriteria relations: Feature relations were analyzed across the entire dataset to identify the most prominent (up to 5%) gait features exhibiting strong consonance (i.e., statistical agreement or dependence).
2. Group-specific intercriteria relations: The analysis was performed separately within each subject group (CONTROL, ALS, HUNT, and PARK) followed by pairwise comparisons between the CONTROL and each NDD group (CONTROL vs. ALS; CONTROL vs. HUNT; CONTROL vs. PARK). Our focus was to identify feature relations presenting strong positive or negative consonance that are unique either to the CONTROL group or to a specific neurodegenerative disorder.

3.2. Population-Level Intercriteria Relations

The exploratory analysis of the 41 defined gait features (C1–C41) across all 14,580 steps in the database using ICrA produced a $\langle \mu, \nu \rangle$ matrix of 41 × 41 dimensions (Figure 5a), containing information for 820 criterion pairs $(41 \times 40)/2$. The $\langle \mu, \nu \rangle$ values are distributed according to the principle illustrated in Figure 3 (left) and visualized as a heatmap, with a color gradient representing positive (green) and negative (red) consonance; a higher color density corresponds to stronger consonance. Although the matrix exhibits distinct patterns of feature relationships, it is difficult to directly select the most prominent pairs due to overlapping and subtle color variations.



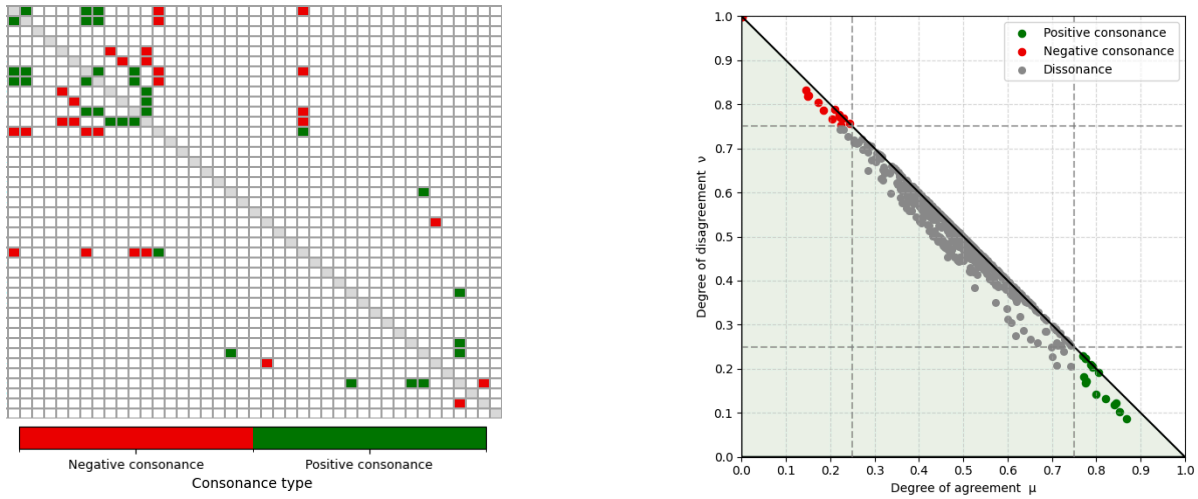
(**a**) (**b**)

Figure 5. Population-level intercriteria relations and threshold sensitivity. (**a**) Heatmap of the $\langle \mu, \nu \rangle$ matrix for 41 gait features (820 criterion pairs), with the green scale indicating positive consonance and red scale indicating negative consonance; a higher color density corresponds to stronger relations. The main diagonal is shown in gray and represents self-relations, which are not evaluated. (**b**) Sensitivity analysis showing the proportion of positively consonant pairs as α/β thresholds vary. The horizontal line marks the 5% selection criterion, with $\alpha = 0.75/\beta = 0.25$ identifying the strongest, most prominent relations (threshold marked with *).

A sensitivity analysis (Figure 5b) was performed to determine the α/β thresholds for identifying strongly consonant pairs. Thresholds were varied from 0 to 1 in steps of 0.05. The proportion of positively consonant feature pairs increased progressively as α was relaxed: very strict thresholds ($\alpha \geq 0.9$) yielded fewer than 0.3% of pairs classified as consonant, while the proportion rose steeply beyond $\alpha \approx 0.7$. The threshold $\alpha = 0.75/\beta = 0.25$ corresponded to 3.66% of all criterion pairs (30 of 820), satisfying the predefined criterion of retaining no more than 5% of the strongest intercriteria relations. Lower thresholds ($\alpha \leq 0.7$) exceeded this limit (>7% of pairs), and thresholds below 0.6/0.4 resulted in the majority of pairs being classified as consonant (≥20%), with $\alpha \leq 0.5$ producing near-complete saturation (≥92%). Based on this analysis, $\alpha = 0.75$ and $\beta = 0.25$ were selected as conservative yet informative thresholds, consistent with the principle that ICrA thresholds should be tuned to shortlist only the most prominent relationships.

Applying these thresholds to the matrix in Figure 5a yielded the filtered $\langle \mu, \nu \rangle$ matrix shown in Figure 6a, with 16 feature pairs exhibiting the strongest positive consonance and 14 exhibiting the strongest negative consonance. For completeness, the fuzzy interpretation triangle is presented in Figure 6b, highlighting the regions of interest in the bottom-right and top-left corners. Feature pairs in the dissonance region were excluded, as these relationships are weak or absent and therefore not relevant for this exploratory analysis of

strong gait relations. The selected strongly consonant pairs are listed in Table 4, including the corresponding feature names and their computed μ and ν values. These relationships, which are of particular interest, are further discussed in the Section 4.



(**a**) (**b**)

Figure 6. Strongly consonant gait-feature relations identified using the ICrA thresholds ($\alpha = 0.75$; $\beta = 0.25$ represented with dotted lines) for features C1–C41 in the population-level: (**a**) filtered $\langle \mu, \nu \rangle$ matrix showing only the feature pairs with strongest positive (green) and negative (red) consonance. White cells correspond to dissonant pairs (i.e., relations without strong consonance). The main diagonal is shown in gray and represents self-relations, which are not evaluated. (**b**) Intuitionistic fuzzy interpretation triangle illustrating all ICrA $\langle \mu, \nu \rangle$ computations and highlighting those pairs that fall within the regions of strong positive and negative consonance.

Table 4. Strongly consonant gait feature pairs at the population level identified by ICrA. The ordered $\langle \mu, \nu \rangle$ values satisfy the conditions for positive consonance ($\mu \geq 0.75$ and $\nu \leq 0.25$) or negative consonance ($\mu \leq 0.25$ and $\nu \geq 0.75$). For each relation, the two gait features forming the criterion pair and their corresponding μ and ν values are listed.

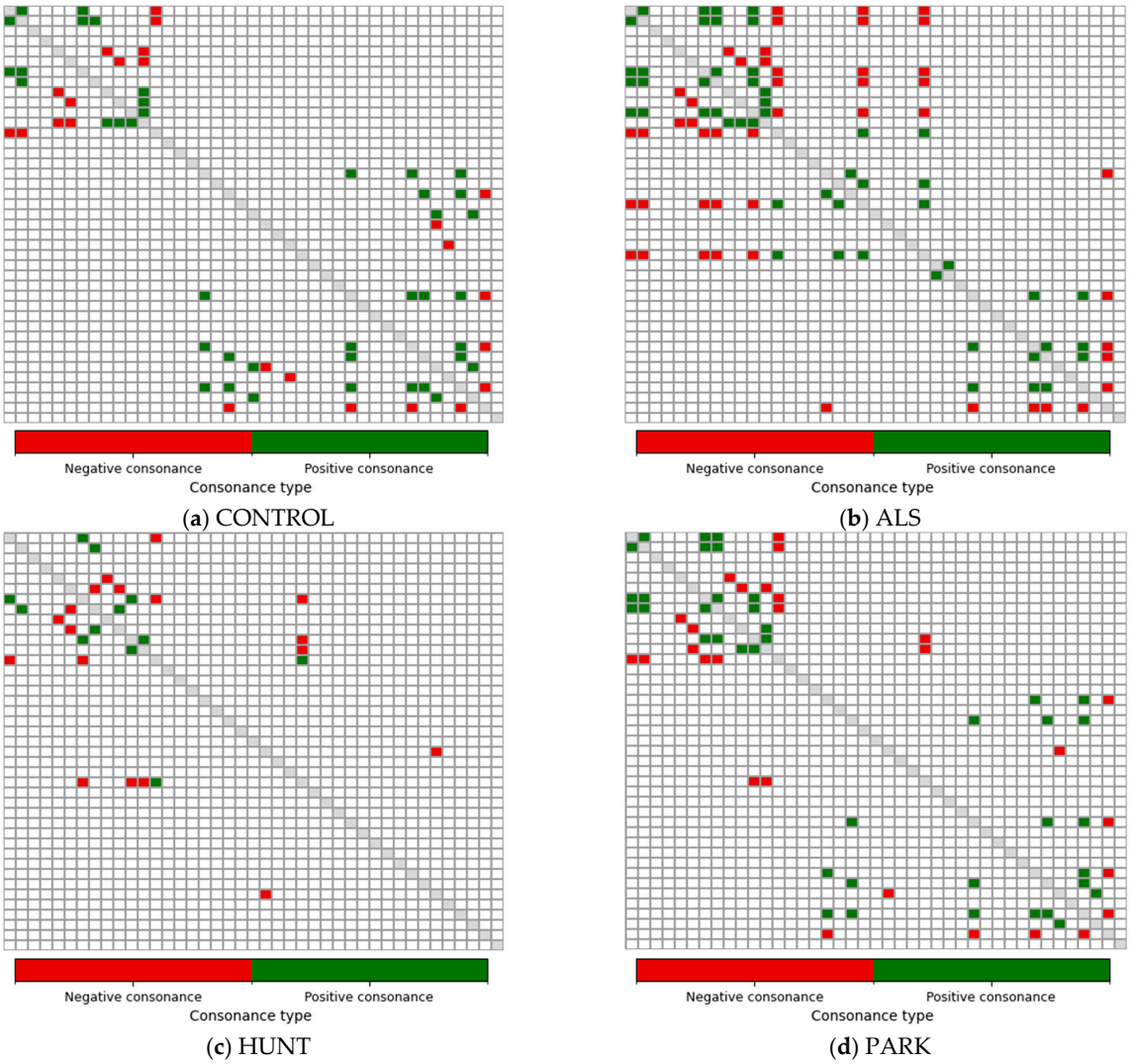
ICrA Result	**ICrA Criteria Pairs Formed by Two Gait Features**		**ICrA Ordered Pair**	
Relation	**Gait Feature 1**	**Gait Feature 2**	μ	ν
Positive Consonance	C01: *LStrInt (s)*	C02: *RStrInt (s)*	0.84	0.12
	C01: *LStrInt (s)*	C07: *LStanInt (s)*	0.87	0.09
	C01: *LStrInt (s)*	C08: *RStanInt (s)*	0.77	0.18
	C02: *RStrInt (s)*	C07: *LStanInt (s)*	0.82	0.13
	C02: *RStrInt (s)*	C08: *RStanInt (s)*	0.85	0.10
	C07: *LStanInt (s)*	C08: *RStanInt (s)*	0.78	0.17
	C07: *LStanInt (s)*	C11: *DSupInt (s)*	0.80	0.14
	C08: *RStanInt (s)*	C11: *DSupInt (s)*	0.78	0.17
	C09: *LStanInt (% stride)*	C12: *DSupInt (% stride)*	0.77	0.23
	C10: *RStanInt (% stride)*	C12: *DSupInt (% stride)*	0.79	0.21
	C11: *DSupInt (s)*	C12: *DSupInt (% stride)*	0.84	0.12
	C13: *Cadance (steps/minute)*	C25: *DSup_RFDavg*	0.77	0.22
	C19: *RStan_RFDmax*	C35: *R_RFDmax(stance-swing)%*	0.77	0.22
	C29: *CorLR_RFD(maxlag)*	C38: *RFDmax(stance-swing)%*	0.79	0.20
	C34: *L_RFDmax(stance-swing)%*	C38: *RFDmax(stance-swing)%*	0.79	0.21
	C35: *R_RFDmax(stance-swing)%*	C38: *RFDmax(stance-swing)%*	0.81	0.19
Negative Consonance	C01: *LStrInt (s)*	C13: *Cadance (steps/minute)*	0.14	0.83
	C01: *LStrInt (s)*	C25: *DSup_RFDavg*	0.22	0.75
	C02: *RStrInt (s)*	C13: *Cadance (steps/minute)*	0.17	0.80
	C05: *LSwInt (% stride)*	C09: *LStanInt (% stride)*	0.00	1.00
	C05: *LSwInt (% stride)*	C12: *DSupInt (% stride)*	0.23	0.77
	C06: *RSwInt (% stride)*	C10: *RStanInt (% stride)*	0.00	1.00
	C06: *RSwInt (% stride)*	C12: *DSupInt (% stride)*	0.21	0.79
	C07: *LStanInt (s)*	C13: *Cadance (steps/minute)*	0.15	0.82
	C07: *LStanInt (s)*	C25: *DSup_RFDavg*	0.18	0.79
	C08: *RStanInt (s)*	C13: *Cadance (steps/minute)*	0.21	0.77
	C11: *DSupInt (s)*	C25: *DSup_RFDavg*	0.15	0.82
	C12: *DSupInt (% stride)*	C25: *DSup_RFDavg*	0.24	0.76
	C22: *LSw_RFDavg*	C36: *L_RFDavg(stance-swing)%*	0.22	0.78
	C38: *RFDmax(stance-swing)%*	C40: *DSup_to_Stan_RFD%*	0.22	0.77

3.3. Group-Specific Intercriteria Relations

To investigate how gait coordination differs between healthy individuals and those with neurological disorders, we applied ICrA to C1–C41 features separately in the CONTROL, ALS, HUNT, and PARK groups. Figure 7 highlights only the strongly consonant gait-feature relations identified using the thresholds derived from the total-population sensitivity analysis ($\alpha = 0.75$; $\beta = 0.25$). The proportion of feature pairs classified as consonant under this criterion was as follows:

- CONTROL group: 3.9% (32 of 820 pairs), 20 positive and 12 negative consonances;
- ALS group: 5.98% (49 of 820 pairs), 25 positive and 24 negative consonances;
- HUNT group: 1.83% (15 of 820 pairs), 6 positive and 9 negative consonances;
- PARK group: 4.15% (34 of 820 pairs), 20 positive and 14 negative consonances;

These values are broadly consistent with the prevalence observed for the total population (3.66%) in Figure 6a, indicating that a similar level of relational selectivity was maintained across all groups.



(**a**) CONTROL (**b**) ALS

(**c**) HUNT (**d**) PARK

Figure 7. Strongly consonant gait-feature relations identified using the ICrA thresholds ($\alpha = 0.75$; $\beta = 0.25$) for features C1–C41 in the four groups: (**a**) CONTROL; (**b**) ALS; (**c**) HUNT; (**d**) PARK. Highlighted cells denote feature pairs with strong positive consonance (green) or strong negative consonance (red). White cells correspond to dissonant pairs (i.e., relations without strong consonance). The main diagonal is shown in gray and represents self-relations, which are not evaluated.

In the present work, however, our focus was not on the absolute coordination patterns within each group displayed in Figure 7, but specifically on group-specific consonances, i.e., intercriteria relations that appear in one group but are absent in the other. For each NDD group (ALS, HUNT, PARK), we compare its ICrA results to those of the CONTROL group and identify the following:

1. Positive consonances present only in one group ($\mu \geq 0.75$ and $\upsilon \leq 0.25$);
2. Negative consonances present only in one group ($\mu \leq 0.25$ and $\upsilon \geq 0.75$),
3. Pairs that satisfy either of the above two conditions and additionally show a substantial between-group difference, defined as follows: $|\mu_\text{CONTROL} - \mu_\text{NDD}| \geq 0.1$ and $|\upsilon_\text{CONTROL} - \upsilon_\text{NDD}| \geq 0.1$.

These criteria allowed us to isolate the relational features of gait that most clearly differentiate healthy coordination from disease-specific alterations.

The resulting group-specific ICrA relations are summarized in the following:

- Table 5 (15 positive consonances) and Table 6 (11 negative consonances) for ALS vs. CONTROL;
- Table 7 (11 positive consonances) and Table 8 (7 negative consonances) for HUNT vs. CONTROL;
- Table 9 (1 positive consonance) and Table 10 (2 negative consonances) for PARK vs. CONTROL.

Table 5. Highlighted gait feature pairs, which present positive consonance (+Cons) only in one of the compared groups (CONTROL vs. ALS). Results from ICrA (ordered pair $\langle \mu, \nu \rangle$) satisfy the +Cons condition ($\mu \geq 0.75$ and $\upsilon \leq 0.25$) in one of the groups (Y: satisfied, N: not satisfied).

ICrA Criteria Pairs Formed by Two Gait Features		**CONTROL**			**ALS**		
Gait Feature 1	**Gait Feature 2**	μ	υ	**+Cons**	μ	υ	**+Cons**
C01: *LStrInt (s)*	C08: *RStanInt (s)*	0.74	0.16 *	N	0.85 *	0.11 *	Y
C01: *LStrInt (s)*	C11: *DSupInt (s)*	0.59	0.30	N	0.78 *	0.16 *	Y
C02: *RStrInt (s)*	C11: *DSupInt (s)*	0.57	0.32	N	0.76 *	0.18 *	Y
C07: *LStanInt (s)*	C08: *RStanInt (s)*	0.72	0.17 *	N	0.84 *	0.11 *	Y
C07: *LStanInt (s)*	C11: *DSupInt (s)*	0.69	0.19 *	N	0.82 *	0.12 *	Y
C08: *RStanInt (s)*	C11: *DSupInt (s)*	0.68	0.20 *	N	0.80 *	0.14 *	Y
C13: *Cadance (steps/minute)*	C20: *RSw_RFDmax*	0.58	0.42	N	0.77 *	0.23 *	Y
C18: *LSw_RFDmax*	C20: *RSw_RFDmax*	0.57	0.43	N	0.79 *	0.21 *	Y
C18: *LSw_RFDmax*	C25: *DSup_RFDavg*	0.64	0.36	N	0.75 *	0.25 *	Y
C20: *RSw_RFDmax*	C25: *DSup_RFDavg*	0.51	0.49	N	0.79 *	0.21 *	Y
C26: *CorLR_F(lag0)*	C27: *CorLR_RFD(lag0)*	0.68	0.31	N	0.84 *	0.16 *	Y
C19: *RStan_RFDmax*	C35: *R_RFDmax(stance-swing)%*	0.83 *	0.17 *	Y	0.70	0.30	N
C19: *RStan_RFDmax*	C38: *RFDmax(stance-swing)%*	0.80 *	0.20 *	Y	0.65	0.34	N
C21: *LStan_RFDavg*	C39: *RFDavg(stance-swing)%*	0.76 *	0.24 *	Y	0.62	0.38	N
C36: *L_RFDavg(stance-swing)%*	C39: *RFDavg(stance-swing)%*	0.75 *	0.25 *	Y	0.65	0.34	N

*: μ or υ satisfy the +Cons condition.

Table 6. Highlighted gait feature pairs, which present negative consonance (–Cons) only in one of the compared groups (CONTROL vs. ALS). Results from ICrA (ordered pair $\langle \mu, \nu \rangle$) satisfy the –Cons condition ($\mu \leq 0.25$ and $\upsilon \geq 0.75$) in one of the groups (Y: satisfied, N: not satisfied).

ICrA Criteria Pairs Formed by Two Gait Features		**CONTROL**			**ALS**		
Gait Feature 1	**Gait Feature 2**	μ	υ	**–Cons**	μ	υ	**–Cons**
C02: *RStrInt (s)*	C20: *RSw_RFDmax*	0.38	0.57	N	0.22 *	0.76 *	Y
C02: *RStrInt (s)*	C25: *DSup_RFDavg*	0.27	0.68	N	0.20 *	0.78 *	Y
C07: *LStanInt (s)*	C13: *Cadance (steps/minute)*	0.21 *	0.72	N	0.15 *	0.81 *	Y
C07: *LStanInt (s)*	C20: *RSw_RFDmax*	0.42	0.51	N	0.21 *	0.76 *	Y
C08: *RStanInt (s)*	C13: *Cadance (steps/minute)*	0.22 *	0.71	N	0.14 *	0.83 *	Y
C08: *RStanInt (s)*	C20: *RSw_RFDmax*	0.36	0.57	N	0.19 *	0.78 *	Y
C11: *DSupInt (s)*	C13: *Cadance (steps/minute)*	0.38	0.54	N	0.20 *	0.76 *	Y
C11: *DSupInt (s)*	C20: *RSw_RFDmax*	0.42	0.51	N	0.19 *	0.77 *	Y
C11: *DSupInt (s)*	C25: *DSup_RFDavg*	0.21 *	0.71	N	0.15 *	0.81 *	Y
C22: *LSw_RFDavg*	C36: *L_RFDavg(stance-swing)%*	0.22 *	0.78 *	Y	0.31	0.68	N
C24: *RSw_RFDavg*	C37: *R_RFDavg(stance-swing)%*	0.21 *	0.78 *	Y	0.35	0.65	N

*: μ or υ satisfy the –Cons condition.

Table 7. Highlighted gait feature pairs, which present positive consonance (+Cons) only in one of the compared groups (CONTROL vs. HUNT). Results from ICrA (ordered pair $\langle \mu, \nu \rangle$) satisfy the +Cons condition ($\mu \geq 0.75$ and $\upsilon \leq 0.25$) in one of the groups (Y: satisfied, N: not satisfied).

ICrA Criteria Pairs Formed by Two Gait Features		CONTROL			HUNT		
Gait Feature 1	**Gait Feature 2**	μ	υ	**+Cons**	μ	υ	**+Cons**
C08: *RStanInt (s)*	C10: *RStanInt (% stride)*	0.59	0.34	N	0.75 *	0.22 *	Y
C01: *LStrInt (s)*	C02: *RStrInt (s)*	0.85 *	0.07 *	Y	0.74	0.22 *	N
C29: *CorLR_RFD (maxlag)*	C17: *LStan_RFDmax*	0.79 *	0.21 *	Y	0.57	0.43	N
C38: *RFDmax(stance-swing)%*	C17: *LStan_RFDmax*	0.76 *	0.24 *	Y	0.60	0.40	N
C38: *RFDmax(stance-swing)%*	C19: *RStan_RFDmax*	0.80 *	0.20 *	Y	0.66	0.34	N
C21: *LStan_RFDavg*	C36: *L_RFDavg(stance-swing)%*	0.76 *	0.24 *	Y	0.66	0.34	N
C29: *CorLR_RFD(maxlag)*	C34: *L_RFDmax(stance-swing)%*	0.80 *	0.19 *	Y	0.60	0.40	N
C29: *CorLR_RFD(maxlag)*	C34: *R_RFDmax(stance-swing)%*	0.77 *	0.22 *	Y	0.66	0.34	N
C38: *RFDmax(stance-swing)%*	C29: *CorLR_RFD(maxlag)*	0.84 *	0.16 *	Y	0.73	0.26	N
C38: *RFDmax(stance-swing)%*	C34: *L_RFDmax(stance-swing)%*	0.84 *	0.16 *	Y	0.69	0.30	N
C38: *RFDmax(stance-swing)%*	C35: *R_RFDmax(stance-swing)%*	0.85 *	0.15 *	Y	0.74	0.26	N

*: μ or υ satisfy the +Cons condition.

Table 8. Highlighted gait feature pairs, which present negative consonance (–Cons) only in one of the compared groups (CONTROL vs. HUNT). Results from ICrA (ordered pair $\langle \mu, \nu \rangle$) satisfy the –Cons condition ($\mu \leq 0.25$ and $\upsilon \geq 0.75$) in one of the groups (Y: satisfied, N: not satisfied).

ICrA Criteria Pairs Formed by Two Gait Features		CONTROL			HUNT		
Gait Feature 1	**Gait Feature 2**	μ	υ	**–Cons**	μ	υ	**–Cons**
C02: *RStrInt (s)*	C13: *Cadance (steps/minute)*	0.14 *	0.82 *	Y	0.28	0.70	N
C06: *RSwInt (% stride)*	C08: *RStanInt (s)*	0.34	0.59	N	0.22 *	0.75 *	Y
C12: *DSupInt (% stride)*	C25: *DSup_RFDavg*	0.34	0.65	N	0.24 *	0.76 *	Y
C19: *RStan_RFDmax*	C40: *DSup_to_Stan_RFD%*	0.22 *	0.77 *	Y	0.34	0.65	N
C22: *RSw_RFDavg*	C37: *R_RFDavg(stance-swing)%*	0.21 *	0.78 *	Y	0.39	0.61	N
C29: *CorLR_RFD (maxlag)*	C40: *DSup_to_Stan_RFD%*	0.24 *	0.75 *	Y	0.38	0.61	N
C34: *L_RFDmax(stance-swing)%*	C40: *DSup_to_Stan_RFD%*	0.22 *	0.77 *	Y	0.40	0.59	N

*: μ or υ satisfy the –Cons condition.

Table 9. Highlighted gait feature pairs, which present positive consonance (+Cons) only in one of the compared groups (CONTROL vs. PARK). Results from ICrA (ordered pair $\langle \mu, \nu \rangle$) satisfy the +Cons condition ($\mu \geq 0.75$ and $\upsilon \leq 0.25$) in one of the groups (Y: satisfied, N: not satisfied).

ICrA Criteria Pairs Formed by Two Gait Features		CONTROL			PARK		
Gait Feature 1	**Gait Feature 2**	μ	υ	**+Cons**	μ	υ	**+Cons**
C08: *RStanInt (s)*	C11: *DSupInt (s)*	0.68	0.20 *	N	0.78 *	0.16 *	Y

*: μ or υ satisfy the +Cons condition.

Table 10. Highlighted gait feature pairs, which present negative consonance (–Cons) only in one of the compared groups (CONTROL vs. PARK). Results from ICrA (ordered pair $\langle \mu, \nu \rangle$) satisfy the –Cons condition ($\mu \leq 0.25$ and $\upsilon \geq 0.75$) in one of the groups (Y: satisfied, N: not satisfied).

ICrA Criteria Pairs Formed by Two Gait Features		CONTROL			PARK		
Gait Feature 1	**Gait Feature 2**	μ	υ	**–Cons**	μ	υ	**–Cons**
C11: *DSupInt (s)*	C25: *DSup_RFDavg*	0.21 *	0.71	N	0.15 *	0.82 *	Y
C12: *DSupInt (% stride)*	C25: *DSup_RFDavg*	0.34	0.65	N	0.25 *	0.75 *	Y

*: μ or υ satisfy the –Cons condition.

These relationships, particularly those that appear uniquely in a given NDD group, form the basis for the clinical interpretations presented in the Discussion.

To assess whether the clinical status or a demographic imbalance influenced the observed relational gait structure, supplementary ICrA analyses were performed, including disease-severity indices (Table S1) and gender (Table S2), according to the results in Supplementary Material S1. Relations between the measured 41 gait features and the available disease-severity scales in the GNDD database (Hoehn and Yahr score for Parkinson's disease, total functional capacity for Huntington's disease, and time since diagnosis for ALS)

were found to be predominantly dissonant. Similarly, the relations between gender and individual gait features also showed dissonance with substantial uncertainty, consistent with the binary nature of the gender variable and the lack of systematic influence on the coordination structure. Together, these findings suggest that the reported ICrA patterns primarily reflect inter-feature organization rather than demographic or severity-driven effects.

3.4. Benchmarking Population-Level Intercriteria Relations Against Reference Correlation Method

To benchmark the intercriteria relations identified by ICrA against a conventional statistical approach, we performed a systematic comparison with a Pearson correlation analysis, which is widely used to quantify linear associations between continuous variables and serves here as a reference method.

The standard ICrA output consists of ordered agreement–disagreement pairs $(\mu, \nu) \in [0; 1]$, reported above and below the main diagonal of the intercriteria matrix (Figure 3). To enable a direct comparison with Pearson correlation coefficients, we introduced a normalization procedure that maps the ICrA outputs onto a symmetric, correlation-like scale in the interval $[-1, 1]$. This transformation produces a normalized ICrA correlation coefficient matrix C^{ICrA}, which is directly comparable, element by element, with the symmetric Pearson correlation matrix $C^{Pearson}$. The normalization preserves the semantic interpretation of ICrA, whereby large positive values indicate strong positive consonance, large negative values indicate strong negative consonance, and values near zero correspond to weak or indeterminate relations. Full details of the normalization procedure are provided in Supplementary Material S1.

Benchmarking was performed at several complementary levels using the complete set of C1–C41 gait feature relations computed over the total population of the GNDD database (the data in Section 3.2). First, the matrices C^{ICrA} and $C^{Pearson}$ were visualized as paired heatmaps on the same color scale $[-1, 1]$. As shown in Figure S1, both matrices exhibit highly similar inter-feature patterns, with only minor, feature-specific differences in color intensity.

Second, the quantitative relationship between the two matrices was assessed through linear regression across all unique feature pairs (Figure S2). The normalized ICrA coefficients show strong linear association with Pearson correlation coefficients (slope = 0.821, 95% CI [0.797–0.845], $R^2 = 0.847$, $p < 0.001$), indicating that ICrA reliably captures the dominant linear dependencies among gait features, while exhibiting a slightly attenuated response for the strongest correlations.

Third, feature-wise differences between normalized ICrA and Pearson correlation coefficients were computed to examine systematic deviations and dispersion across gait features (Table S3). Across all features, the mean difference is close to zero (-0.014) with moderate dispersion (0.088), demonstrating strong overall agreement between the two measures. The small negative bias reflects the conservative nature of the ICrA framework, in which uncertainty component moderates the magnitude of the normalized coefficients relative to Pearson correlation.

Finally, the strongly consonant gait feature pairs identified by ICrA (Table 4) were further examined by augmenting their $\langle \mu, \nu \rangle$ values with the corresponding normalized ICrA and Pearson correlation coefficients (Table S4). All selected pairs exhibit highly significant Pearson correlations ($p < 0.001$), with strong positive or negative associations (absolute values ranging from 0.46 to 1.00), further confirming the consistency between ICrA-derived relations and the conventional correlation analysis.

Overall, this benchmarking framework validates the ICrA-derived intercriteria relations against a classical multivariate statistical measure, demonstrating that ICrA captures

conventional linear dependencies while providing additional interpretive insight through its explicit representation of agreement, disagreement, and uncertainty.

4. Discussion

The first major contribution of this study is the construction of a high-dimensional gait dataset comprising 41 temporal and kinetic features derived from the ground reaction force signal and its rate of force development. The features were computed with explicit attention to laterality (left/right leg), phase-dependent dynamics (stance, swing, and double support), and multiple forms of biomechanical organization, including magnitude-based descriptors, waveform correlations, and inter- and intra-limb asymmetries. This results in a comprehensive representation of gait that captures both the timing structure of the gait cycle and the neuromechanical properties of force production.

Some degree of feature redundancy is inherent to the proposed descriptor set, as multiple temporal and kinetic measures reflect related biomechanical and neuromuscular processes. This redundancy was intentionally preserved, since the InterCriteria Analysis framework evaluates patterns of inter-feature relationships rather than isolated descriptors. Features with overlapping physiological meaning may nonetheless exhibit distinct relational behavior in pathological gait, providing additional insight into altered coordination mechanisms.

Furthermore, the present study is, to our knowledge, the first to apply the full analytical power of the ICrA framework to examine the relational patterns within such a high dimensional gait dataset. Unlike conventional statistical or machine-learning approaches that primarily quantify differences in feature magnitudes, ICrA characterizes the relational structure among features through intuitionistic fuzzy intercriteria relations. Importantly, no machine-learning or deep-learning models were employed in this study. The analysis is explicitly exploratory in nature: rather than developing or validating a diagnostic or predictive model, ICrA is used to examine how multiple gait features co-vary and form coordination patterns that distinguish healthy from pathological gait. This enables an examination of gait as a multivariate, interdependent system, where coordination patterns are encoded not only in individual feature values but also in the configuration of positive and negative consonances linking them. These relational patterns describe associations between gait features rather than causal relationships, and all interpretations should therefore be regarded as exploratory. By applying ICrA at both the population level and in comparisons between the CONTROL group and each NDD group, we sought to identify relational gait patterns that are either preserved across all subjects or selectively disrupted in ALS, Huntington's disease, and Parkinson's disease.

In this study, ICrA was applied as an established analytical framework rather than extended methodologically. The procedure was implemented exactly as provided in the ICrAData software, without modification of the underlying theory, algorithms, or parameterization. Our contribution therefore lies in the systematic application of ICrA to a high-dimensional gait dataset and in the interpretation of the resulting relational structures, rather than in proposing theoretical developments of the method itself.

The analyses were conducted using a single publicly available dataset (GNDD, PhysioNet). Given the rarity of large repositories containing force-sensor gait recordings across multiple neurodegenerative disorders, no external dataset with comparable structure and diagnostic representation was available for replication. Accordingly, the present work should be regarded as an exploratory investigation of inter-feature relational structure rather than a validation study or model-performance evaluation. Within this exploratory context, the key strength of the ICrA approach lies in its ability to detect group-specific consonances—intercriteria relations that appear only in one group and not in another.

These unique relational patterns may reflect structural changes in gait organization that cannot be uncovered through traditional single-feature or pairwise statistical analyses.

In line with published ICrA methodology, consonance thresholds were not chosen arbitrarily but were instead tuned to retain approximately the top 5% of the strongest intercriteria relations. A sensitivity analysis confirmed that the adopted thresholds ($\alpha = 0.75$; $\beta = 0.25$) were the highest values that still satisfied this predefined retention criterion. Importantly, the proportion of retained pairs within each diagnostic group was broadly consistent with the population-level value (≈3.7%), indicating that a comparable level of relational selectivity was maintained across analyses. This procedure enhances the interpretability of the resulting feature-relation maps while also supporting the robustness of the main conclusions with respect to reasonable variations in threshold choice.

It should be noted that the majority of feature pairs exhibit dissonance or weak associations, which are not discussed individually. These dissonant relationships primarily reflect the absence of systematic coupling and are expected in a high-dimensional dataset of 41 gait features, resulting in over 800 pairwise combinations. By focusing on the top ~5% strongest consonances, the analysis highlights the most robust coordination patterns that are most relevant for understanding disease-specific alterations in gait, without over-interpreting noise or spurious relationships.

To further validate the extracted consonances, the ICrA-derived intercriteria relations were benchmarked against the Pearson correlation analysis. The strong linear association between the normalized ICrA correlation coefficients and Pearson correlations ($R^2 = 0.847$, $p < 0.001$) demonstrates that ICrA reliably captures dominant linear dependencies among gait features. The slight systematic underestimation of correlation strength reflects the conservative nature of the ICrA framework, in which uncertainty moderates the magnitude of inferred relations. Thus, ICrA recovers a conventional correlation structure while providing an enriched representation through its explicit agreement–disagreement formalism.

The following subsections discuss these findings at the population level (Section 4.1) and in the context of group-specific distinctions (Section 4.2). Because ICrA focuses on relational patterns among multiple gait features rather than single-feature effect sizes, a descriptive narrative is necessary to convey the structure, directionality, and group-specific relevance of the observed consonances. This approach ensures that complex inter-feature coordination and its clinical interpretation are communicated clearly.

4.1. Population-Level Intercriteria Relations

An analysis of the entire population using the ICrA in Table 4 revealed patterns of strong positive and negative consonance between gait features, providing insights into feature dependencies and relative importance for classification tasks. Figure 8 illustrates the number of consonance pairs in which each feature participates, highlighting the most interconnected gait parameters across the dataset.

According to Figure 8, several features emerged as highly representative, participating in multiple consonance pairs. Among temporal features, the left stance interval *LStanInt (s)* and double-support interval expressed as a percentage of stride *DSupInt (% stride)* appear in six pairs each, indicating strong interdependence with other stride-to-stride features. The right stance interval *RStanInt (s)*, left stride interval *LStrInt (s)*, cadence, and average RFD during double support *DSup_RFDavg* are each involved in five pairs, also demonstrating substantial connectivity. These features likely capture fundamental aspects of gait dynamics, including the stance-phase duration, bilateral coordination, and timing of weight transfer, making them particularly informative when selecting a reduced feature set.

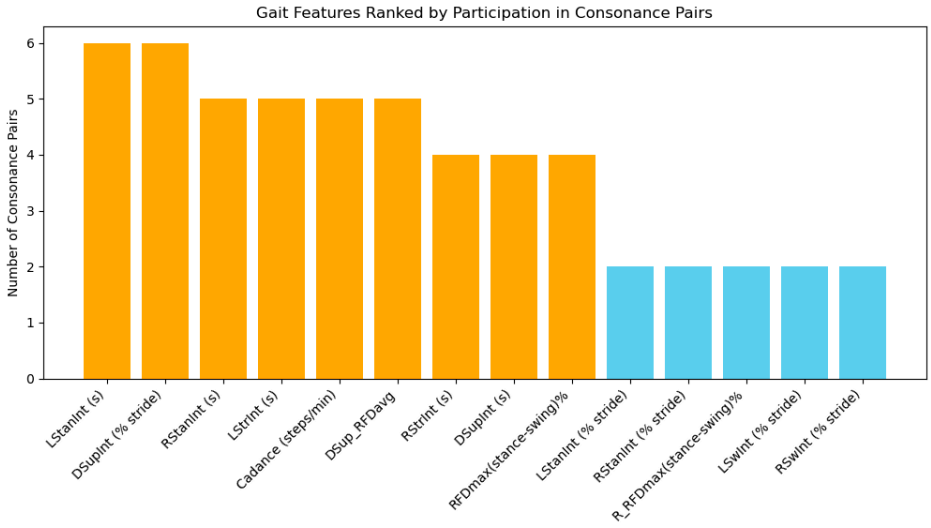


Figure 8. Number of consonance pairs for each gait feature calculated from the Gait in Neurodegenerative Disease Database using ICrA, accounted from Table 4. Features involved in four or more pairs are highlighted in orange, indicating high representativeness and potential priority for inclusion in a reduced feature set for NDD classification. Features involved in fewer than four pairs are shown in blue, suggesting lower redundancy and potentially unique contributions.

Features participating in four consonance pairs, such as right stride interval *RStrInt (s)*, absolute double-support interval *DSupInt (s)*, and global RFD asymmetry between stance and swing *RFDmax(stance-swing)%*, also contribute important interrelated information, reflecting phase-dependent force generation and stride timing. In contrast, features such as the left and right swing intervals (*LSwInt (s)*, *RSwInt (s)*) appear in few or no high-consonance pairs, suggesting that they carry unique, independent information that may be crucial for NDD classification despite their lower redundancy.

The analysis confirms that temporal features of the step are interdependent, with 10 out of 12 appearing in strong-consonance pairs. This indicates that including all such features in a classifier may lead to redundancy, whereas focusing on the most connected features can reduce dimensionality without significant information loss. Kinetic and derived features, including *DSup_RFDavg*, *RFDmax(stance-swing)%*, and cadence, exhibit moderate to high interconnections, highlighting their relevance for capturing neuromuscular control and bilateral coordination. At the same time, features with limited participation in consonance pairs may provide complementary, independent information, improving classification accuracy by adding unique perspectives on gait dynamics.

4.2. Group-Specific Intercriteria Relations

4.2.1. ALS Patients vs. Healthy Controls

Group-specific analysis using ICrA (Tables 4 and 5) reveals that certain gait features are involved in a higher number of strong consonance pairs within either ALS patients or healthy controls, highlighting features that may be particularly informative for diagnosing this neurodegenerative disorder. By counting the number of group-specific consonances associated with each feature, regardless of whether the relationship is positive or negative, we can identify the features that most strongly distinguish each group (Figure 9). Notably, six temporal features and three kinetic RFD-based features appear repeatedly, each participating in two to seven ALS-specific consonance pairs (orange bars), while none of these relations are present in healthy controls (blue bars). This consistent involvement suggests that these features capture important alterations in neuromuscular control and compensatory strategies characteristic of ALS gait, highlighting their importance for further clinical investigation.

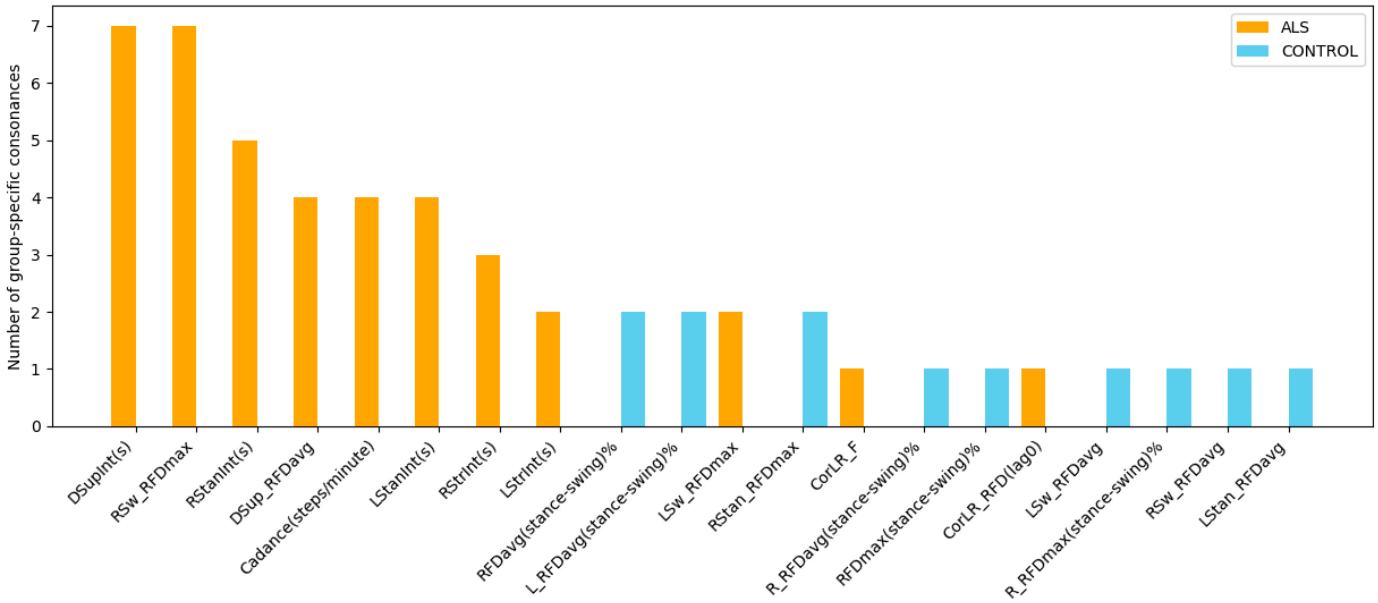


Figure 9. Number of group-specific consonances in gait features for ALS patients (orange) and healthy controls (blue), accounted from Tables 4 and 5. The plot identifies temporal and kinetic gait features that present strong relations in one group but are absent in the other, thereby revealing structural differences in gait coordination between ALS disease and healthy controls.

Further, all temporal and kinetic relationships identified by ICrA as specific to the CONTROL and ALS groups (Tables 4 and 5) are examined below within their clinical context:

- CONTROL-specific consonances between temporal features:
  - a. Positive consonance between *LStrInt(s)* and *RStrInt(s)*: This bilateral dependency reflects stable, symmetric regulation of left- and right-leg stride intervals typical of healthy gait. Its absence in the ALS group corresponds to the well-documented increase in temporal irregularity, impaired step-to-step consistency, and reduced ability to maintain stable rhythm in ALS [15,16].
  - b. Negative consonance between *RStrInt(s)* and *Cadence(steps/minute)*: This inverse relation—longer stride intervals paired with lower cadence—is present in a normal gait. Its absence in ALS patients suggests a pathological decoupling between the stride duration and step rhythm, consistent with reduced walking speed and timing variability associated with neuromuscular weakness [5,7,16].
- ALS-specific consonances between temporal features:
  - a. Positive consonances of *LStrInt(s)*, *RStrInt(s)*, *LStanInt(s)*, *RStanInt(s) vs. DSupInt(s)*: These multiple interdependencies indicate that ALS patients exhibit globally coupled timing patterns across stride, stance, and double-support intervals. Such coupling reflects the characteristic prolongation of stance and overall gait cycle duration due to muscle weakness, instability, and reduced motor control efficiency [16].
  - b. Negative consonances between stance-related intervals (*LStanInt(s)*, *RStanInt(s)*, *DSupInt(s)*) and *Cadence(steps/minute)*: In ALS, increases in stance or double-support duration directly correspond to reduced cadence, highlighting a slowed gait driven by a prolonged weight-bearing time [15–17]. This relation is not present in controls and aligns with compensatory strategies used to maintain stability when limb force generation is compromised.
- CONTROL-specific consonances between kinetic RFD-based features:

a. Positive consonances of *RFDmax(stance–swing)%*, *L_RFDmax(stance–swing)%*, *R_RFDmax(stance–swing)%*, *LStan_RFDmax vs. RStan_RFDmax:* Reflect coordinated bilateral modulation of force production during stance–swing transitions—indicative of efficient neuromuscular control and symmetrical loading in a healthy gait.
b. Positive consonances linking *CorLR_RFD(maxlag)* to *L_RFDmax(stance–swing)%*, *R_RFDmax(stance–swing)%*, *RFDmax(stance–swing)%*, and *LStan_RFDmax*: Demonstrate robust left–right synchronization of force-generation dynamics, reflecting preserved inter-limb coordination in healthy gait. This synchrony is markedly reduced in ALS, where neuromuscular degeneration disrupts the temporal alignment of limb kinetics and leads to desynchronized force-production patterns [80].
c. Positive consonance between *LStan_RFDavg* and *L_RFDavg(stance–swing)%*: Indicates that higher stance-phase RFD is associated with greater overall force-development capacity across the full stance–swing cycle, typical of healthy, well-regulated loading patterns.
d. Negative consonances between corresponding kinetic features of the left and right legs, specifically *LSw_RFDavg* vs. *L_RFDavg(stance–swing)%* and *RSw_RFDavg* vs. *R_RFDavg(stance–swing)%:* Indicate that force development is naturally lower during swing than during stance, consistent with normal biomechanical demands. The absence of these relations in ALS suggests impaired modulation of force across gait phases, reflecting a reduced ability to dynamically regulate limb loading [81].

- ALS-specific consonances between kinetic features:
  a. Positive consonances between *LSw_RFDmax*, *RSw_RFDmax*, and *DSup_RFDavg*: These relations suggest altered coordination of force generation during swing and double-support phases. They reflect compensatory adaptations linked to muscle weakness, reduced hip control, and increased instability characteristic of an ALS gait [15–17].
  b. Positive consonance between *CorLR_F(lag0)* and *CorLR_RFD(lag0)*: Indicates that reductions in bilateral force coordination are closely coupled with the impaired synchronization of RFD. Such coupling is consistent with the ALS-related degeneration of motor-unit recruitment and inter-limb communication [82].
  c. Negative consonances of *RSw_RFDmax* and *DSup_RFDavg* vs. temporal intervals (*RStrInt(s)*, *LStanInt(s)*, *RStanInt(s)*, and *DSupInt(s)*): Show that prolonged stance or double-support phases constrain dynamic force production during swing. These interactions, absent in healthy controls, reflect the tendency of ALS patients to adopt longer support phases [17], while reducing the capacity for rapid force generation in swing.

4.2.2. HUNT Patients vs. Healthy Controls

Comparing the HUNT and CONTROL groups using ICrA revealed group-specific patterns of strong positive and negative consonances between temporal and kinetic gait features, as summarized in Tables 6 and 7. Further, Figure 10 provides a graphical summary of all gait features involved in consonance pairs unique to either CONTROL or HUNT subjects. Most features in consonance belong exclusively to the CONTROL group (blue bars), reflecting a rich and well-preserved coordination structure across temporal and kinetic domains. In contrast, the HUNT group shows only sparse feature involvement (orange bars), indicating a substantial reduction in coordinated inter-feature relationships characteristic of Huntington's disease.

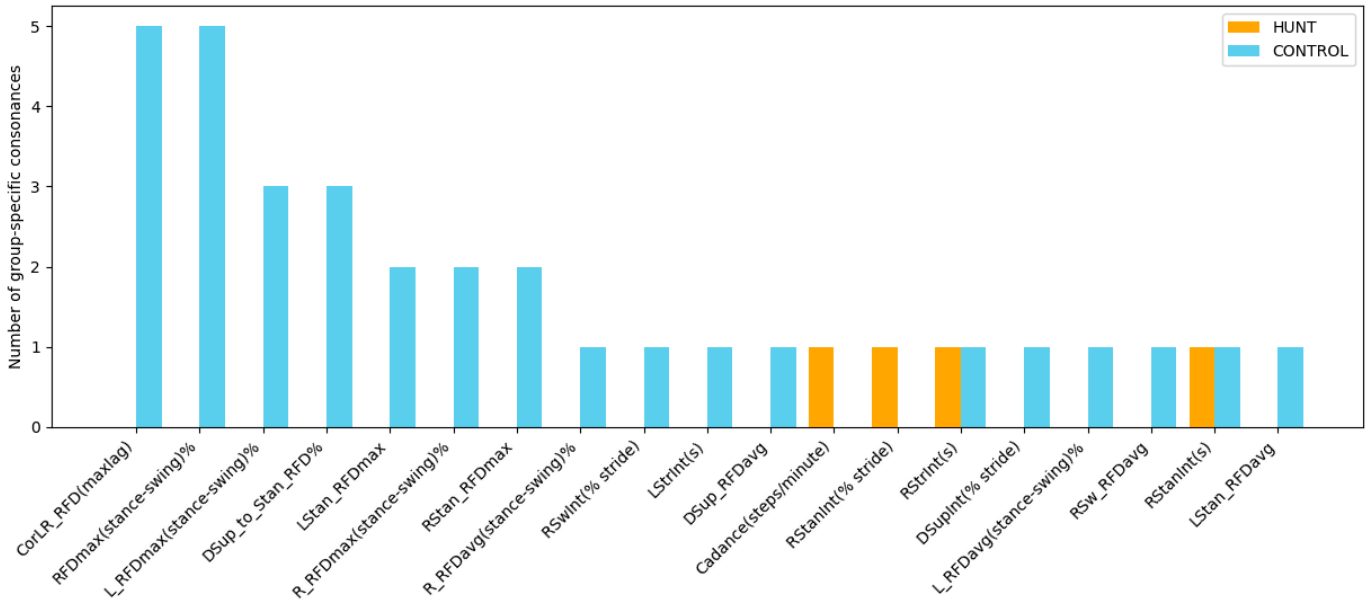


Figure 10. Number of group-specific consonances in gait features for HUNT patients (orange) and healthy controls (blue), accounted from Tables 6 and 7. The plot identifies temporal and kinetic gait features that present strong relations in one group but are absent in the other, thereby revealing structural differences in gait coordination between Huntington's disease and healthy controls.

A detailed analysis of the ICrA results in Tables 6 and 7 highlights several characteristic temporal and kinetic relationships that distinguish the CONTROL and HUNT groups, with the following observations linking these patterns to clinical interpretation:

- CONTROL-specific consonances between temporal features:
  - a. Positive consonance between *LStrInt(s)* and *RStrInt(s)*: This bilateral dependency reflects stable, symmetric regulation of left- and right-leg stride intervals typical of a healthy gait. Its absence in the HUNT group corresponds to well-known Huntington's disease features such as elevated temporal variability, irregular step-to-step transitions, and difficulty in sustaining consistent forward progression [7,13,14].
  - b. Negative consonance between *RStrInt(s)* and *Cadance(steps/minute)*: This inverse relation—longer stride intervals paired with lower cadence—is typical for a normal gait. Its absence in HUNT patients suggests a pathological decoupling between stride duration and stepping rhythm, consistent with irregular pacing and increased stride-timing variability.
- HUNT-specific consonances between temporal features:
  - a. Positive consonance between *RStanInt(s)* and *RStanInt(% stride)*: This indicates that in HUNT patients, the absolute and relative durations of the right stance phase increase proportionally—a dependency consistent with the compensatory lengthening of stance time often reported in individuals with instability, chorea, or fear of falling [83]. This feature is not present in controls, underscoring a disease-specific alteration in stance-phase organization.
  - b. Negative consonance between temporal features *RStanInt(s)* and *RSwInt(% stride)*: Increased stance time corresponds to proportional reductions in swing time. This asymmetrical temporal adjustment is not seen in controls and supports the interpretation that HUNT patients adopt prolonged stance [84] as a compensatory mechanism to maintain stability.
- CONTROL-specific consonances between kinetic RFD variables:

a. Positive consonances among *RFDmax(stance–swing)%*, *L_RFDmax(stance–swing)%*, *R_RFDmax(stance–swing)%*, *LStan_RFDmax*, and *RStan_RFDmax:* Reveal coordinated bilateral modulation of force production during stance–swing transitions—an indicator of intact motor control in healthy gait.
b. Positive consonance linking *CorLR_RFD(maxlag)* to *L_RFDmax(stance–swing)%*, *R_RFDmax(stance–swing)%*, *RFDmax(stance–swing)%*, and *LStan_RFDmax*: Reflects strong left–right synchronization of RFD, further underscoring coordinated bilateral force generation.
c. Positive consonance between *LStan_RFDavg* and *L_RFDavg(stance–swing)%*: Suggests that higher stance-phase RFD corresponds to higher overall force-development capacity across the stance–swing cycle.
d. Negative consonance between *DSup_to_Stan_RFD%* to *RStan_RFDmax*, *CorLR_RFD(maxlag)*, and *L_RFDmax(stance–swing)%:* Indicate efficient redistribution of force from double-support to stance and coordinated inter-limb regulation of loading.
e. Negative consonance between *RSw_RFDavg* and *R_RFDavg(stance–swing)%*: Shows that force development is naturally lower during swing than stance, consistent with expected biomechanical demands of a healthy gait. The absence of these negative kinetic consonances in HUNT suggests disruption in normal load-transfer strategies and impaired modulation of force across gait phases.

- HUNT-specific consonances between temporal and kinetic RFD features:
  a. Negative consonance between *DSupInt(% stride)* and *DSup_RFDavg*: Indicates that longer double-support intervals are associated with reduced force development, suggesting slowed movement, increased stiffness, or a cautious gait strategy characteristic of Huntington's disease [7,13,14].

4.2.3. PARK Patients vs. Healthy Controls

Detailed analysis of the ICrA results in Tables 8 and 9 reveals only a small set of temporal–kinetic relationships that distinguish PARK patients from healthy controls, summarized in Figure 11. Compared with ALS and HUNT, the number of PARK-specific consonances is notably limited, suggesting more subtle alterations in inter-feature coupling.

The identified relations and their clinical interpretation are as follows:

- CONTROL-specific consonances between gait features are not identified, indicating that the distinguishing relations arise exclusively from PARK-specific alterations.
- PARK-specific consonances between temporal and kinetic features:
  a. Positive consonance between *RStanInt(s)* and *DSupInt(s)*: This dependency indicates that in PARK patients, prolongation of the right stance phase is directly associated with increased double-support time. This pattern aligns with characteristic shuffling gait in Parkinson's disease, where feet are insufficiently lifted and weight transfer becomes slower and more prolonged [85]. The absence of this relation in healthy controls suggests that this coupling reflects disease-specific compensation for postural instability and bradykinetic movement.
  b. Negative consonance between *DSupInt(s)* and *DSup_RFDavg*: Longer double-support duration corresponds to reduced force development during double support. This relationship reflects the slow, hesitant, and low-amplitude movements typical of a Parkinsonian gait [8,9], where decreased push-off dynamics and stiffness reduce the force generated during weight transfer.
  c. Negative consonance between *DSupInt(% stride)* and *DSup_RFDavg*: A proportional increase in the relative duration of double support is accompanied by reduced RFD during the same phase. This reinforces the interpretation that

prolonged stabilization phases in Parkinson's disease come at the cost of diminished dynamic force production, consistent with bradykinesia and decreased lower-limb motor drive.

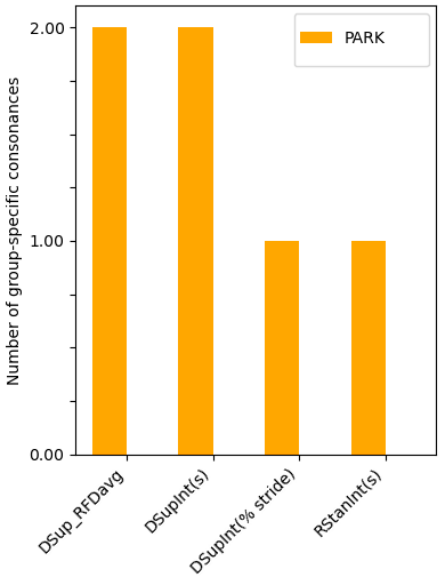


Figure 11. Number of group-specific consonances in gait features for PARK patients (orange) versus healthy controls, with no CONTROL-specific consonances detected (Tables 8 and 9). The plot highlights three temporal and one kinetic feature involved in PARK-unique intercriteria relations, revealing a few structural alterations in gait coordination characteristic of Parkinson's disease.

4.3. Related Work and Comparisons

Despite its limited cohort sizes, the GNDD database has been widely used in gait analysis studies to investigate gait alterations in neurodegenerative disorders relative to healthy controls. Prior work can be broadly categorized according to the methodological strategy used for gait feature representation.

The first category comprises black-box deep-learning approaches, which operate directly on raw GRF signals or their transformed representations. Examples include deep neural networks applied to left- and right-foot GRF time series [86], recurrence plots derived from GRF signals [87], and time–frequency images obtained via wavelet transforms [88–90]. Although such methods often achieve high classification accuracy, their learned representations are difficult to interpret biomechanically, and they provide limited insight into the specific gait mechanisms underlying group differences.

The second category of GNDD-based studies derives gait information from engineered temporal and kinetic features, including combinations of stride timing measures, force amplitudes, variability indices, and statistical descriptors computed from GRF signals and their derivatives, which are subsequently used for supervised classification of NDD patients versus controls [2,16,24,53–55,91–94]. A common methodological choice in this literature is stride-by-stride feature extraction, rather than averaging gait parameters over longer time windows (e.g., 10–60 s) [94]. This strategy, adopted in numerous studies [2,16,24,54,91–93] preserves stride-to-stride variability and transient fluctuations, which are well-established hallmarks of a neurodegenerative gait. The present study follows this established paradigm by representing each individual gait cycle using a 41-dimensional temporal–kinetic feature vector, thereby retaining fine-grained temporal dynamics and neuromechanical information that would be attenuated by stride-averaged representations.

Compared with prior work, the feature set constructed here expands the scope of commonly used descriptors in two main directions. First, in addition to primary temporal

parameters (stride, stance, swing, and double-support intervals), we explicitly incorporate rate-of-force-development features, capturing both peak and average force-derivative amplitudes during stance and swing. While statistical features derived from GRF signals and their derivatives have previously been shown to support high NDD classification accuracy using support vector machines (SVM) and K-nearest neighbors (KNN) classifiers [94], the present study emphasizes the physiological interpretation of RFD as a marker of neuromuscular responsiveness and phase-dependent force modulation, rather than its sole utility for classification.

Several earlier studies have highlighted the diagnostic relevance of temporal features such as the stance duration and double-support intervals [54]. Consistent with these findings, our ICrA analysis reveals strong, group-specific relational patterns involving *DSupInt* and stance-related features, providing a relational explanation for their diagnostic importance beyond univariate feature ranking.

Correlation-based gait descriptors have also been explored in prior work, typically assessed using statistical tests (e.g., tests ANOVA, Kruskal–Wallis), or conventional correlation analysis to identify group differences [16,93]. Although these studies did not report classification performance based on correlation features alone, they demonstrated their sensitivity to pathological gait organization. In agreement with these observations, the present study identifies group-specific consonances involving inter-limb force and RFD correlations, including *CorLR_F* and *CorLR_RFD(lag0)* in ALS and *CorLR_RFD(maxlag)* in HUNT, highlighting disrupted bilateral coordination patterns not readily captured by magnitude-based features alone.

Reported classification accuracies with the primary temporal features provided with the GNDD database vary widely depending on feature selection and classifier choice, ranging as approximately 91–97% for ALS, 78–100% for HUNT, and 79–100% for PARK using classifiers such as SVM, KNN, random forests, multilayer perceptrons, and convolutional neural networks [24,53–55]. Importantly, several studies have shown that feature selection is critical for achieving robust performance. For example, Xia et al. [55] showed that reducing the feature set from 18 to as few as 2–7 features improved classification accuracy from approximately 80% to above 90% using SVM and KNN classifiers, while Prabhu et al. [92] reported accuracy gains of 20–39% after applying hill-climbing feature selection algorithms.

These findings underscore the risk of overfitting associated with high-dimensional feature spaces and motivate the analytical strategy adopted in the present work. Rather than proposing a final classifier, we employ InterCriteria Analysis to identify robust, non-redundant, and physiologically interpretable feature relationships prior to predictive modeling. By revealing which temporal–kinetic features form stable coordination patterns within and across diagnostic groups, ICrA provides a principled basis for subsequent feature selection, supporting future classification studies with improved generalizability, interpretability, and clinical relevance. Conceptually, this relational perspective distinguishes the present work from feature-ranking and classifier-driven approaches that primarily assess individual feature importance. By contrast, ICrA focuses on the structure of inter-feature dependencies, enabling physiologically meaningful coordination patterns to be identified even when individual features exhibit weak univariate effects—an aspect particularly relevant for neurodegenerative gait, where pathology often manifests as altered coordination rather than isolated parameter shifts.

5. Study Limitations

This study used a single publicly available archive (GNDD, PhysioNet). Because no external dataset with a comparable recording modality and diagnostic representation was available, the generalizability of the identified relational structures cannot yet be

confirmed. The work was intended as an exploratory demonstration of ICrA applied to gait, rather than a validation study. Future research using prospectively collected, multi-center datasets—and ideally different sensor systems—is required to test the robustness and clinical relevance of these coordination patterns.

Although subject numbers were modest (CONTROL: 16; ALS: 13; HUNT: 20; PARK: 15), the large number of gait cycles per participant (mean 237 steps per recording) results in a substantial number of feature–pair evaluations (≈11.96 million across the full dataset), which improves the stability and reliability of inter-feature consonance estimates in ICrA. We note, however, that steps within a participant are not fully independent, so the step-level sample size inflates nominal counts. ICrA is an exploratory, relational method focusing on inter-feature coordination rather than classical hypothesis testing, and statistical significance at the participant level is not computed within the framework. Accordingly, our primary analyses emphasize the characterization and interpretation of group-level relational patterns, rather than formal inferential claims. The large number of steps per participant enhances the robustness of feature–pair estimates, while final interpretations are made at the participant-group level, mitigating concerns of inflated inference. Nevertheless, the limited cohort sizes and potential heterogeneity within groups mean that the results should be interpreted as exploratory and descriptive rather than statistically definitive.

Lag values associated with the peak cross-correlation were not analyzed. Although such metrics may provide additional insight into inter-limb timing asymmetry, the present work focused on synchrony-strength measures, which are more robust to cadence variability, waveform distortion, and step-to-step timing irregularity commonly observed in NDD gait.

Finally, the identified relational patterns were not tested against clinical diagnostic outcomes, and their direct predictive or translational value remains to be established.

6. Conclusions

This study introduces an expanded, high-dimensional set of 41 gait-related temporal and kinetic features and applies ICrA to quantify how these parameters relate to one another in both neurodegenerative and healthy populations. By examining the structure of inter-feature consonances, the approach captures not only the global organization of gait across all participants but also the disease-specific coordination patterns characteristic of ALS, Huntington's disease, and Parkinson's disease. The resulting observations can therefore be interpreted at two complementary levels: a population-level view that reveals the overarching hierarchy of dependencies among gait features, and a group-specific view that highlights how neurodegeneration alters these relationships in distinct and clinically meaningful ways.

In summary, the population-level ICrA results reveal a structured hierarchy of inter-feature dependencies, providing a data-driven basis for prioritizing gait features and reducing dimensionality in NDD classification. Core temporal parameters, particularly stance intervals and double-support duration, show the highest consonance participation, reflecting strong redundancy and centrality in gait timing. Stride intervals and cadence also display notable interdependence, highlighting their role in fundamental gait coordination. In contrast, most kinetic and RFD-based variables participate in fewer consonances, indicating that they capture more independent neuromechanical information. These findings suggest that temporal features form the core of gait dynamics, while kinetic features offer complementary, non-redundant information that may enhance classifier sensitivity to subtle neuromuscular impairments. Developing such classifiers represents a potential future perspective.

At the group-specific level, ICrA reveals how temporal and kinetic gait features co-vary differently in neurodegenerative disorders compared with healthy gait, exposing

disease-specific disruptions in neuromuscular coordination, force modulation, and bilateral synchronization. These relational patterns extend beyond differences in individual feature values and highlight how entire subsystems of gait become reorganized in ALS, Huntington's disease, and Parkinson's disease:

- ALS vs. CONTROL: ICrA identifies numerous temporal and kinetic consonances unique to ALS, indicating widespread alterations in the stance duration, stride timing, force-generation dynamics, and RFD modulation. The disrupted relationships observed among stance–swing timing, inter-limb synchronization, and intra-limb RFD asymmetries point to impaired neuromuscular control and compensatory strategies characteristic of an ALS gait. In contrast, controls show coherent bilateral regulation of RFD and consistent coupling between temporal and kinetic features, suggesting preserved coordination mechanisms absent in ALS.
- HUNT vs. CONTROL: HUNT patients show the most pronounced breakdown of relational gait structure. The loss of nearly all control-specific consonances, coupled with the emergence of only a few weak disease-specific dependencies, indicates severe disruption in the timing relationships that normally link stride intervals, stance–swing organization, and force-production patterns. These findings align with the well-known high temporal variability, instability, and irregular step-to-step transitions characteristic of Huntington's disease.
- PARK vs. CONTROL: Compared with ALS and HUNT, Parkinson's disease exhibits only a small number of group-specific consonances. The differences are subtle and largely confined to relationships involving stance duration, double-support timing, and reduced RFD during double support. These limited alterations suggest that inter-feature coordination in a Parkinsonian gait remains mostly preserved, with detectable disruptions reflecting hallmark features such as shuffling, slowed step initiation, and reduced propulsive force.

Across all three disorders, ICrA reveals how neurodegeneration reshapes the interdependent structure of the gait, with ALS and HUNT showing extensive reorganization of temporal–kinetic relationships and PARK exhibiting only localized disruptions. By identifying group-specific positive and negative consonances—relational patterns present or absent relative to healthy gait—ICrA uncovers disease-specific coordination signatures that reflect underlying neuromechanical dysfunction.

It should be emphasized that these findings were derived from a single publicly available PhysioNet archive (GNDD). In the absence of an external dataset with comparable sensor modality and diagnostic composition, the present study should be regarded as an exploratory characterization of inter-feature relational structure rather than a validation study. Future work involving independent, prospectively collected datasets will be required to confirm the stability and generalizability of the coordination patterns reported here. ICrA was applied here as an established analytical framework without modification, and the novelty of the present work therefore lies in its application to a high-dimensional gait dataset and the interpretation of the resulting relational structures. Within this exploratory context, benchmarking against the Pearson correlation demonstrated that the extracted ICrA relations are consistent with conventional linear dependencies, providing methodological support for the reported patterns. In addition to these analytical insights, we also demonstrated that the full workflow is computationally efficient: runtime measurements show that both gait-feature extraction and the ICrA procedure scale approximately linearly with dataset size, indicating that the method is readily applicable to substantially larger gait repositories without modification. While these findings are exploratory and not validated against clinical diagnostic outcomes, they provide a principled basis for future studies aimed at linking gait relational patterns to clinical endpoints and translational applications.

Even within this exploratory context, the results demonstrate that ICrA offers a powerful framework for revealing the latent organization of gait and for distinguishing disorder-specific alterations in neuromechanical coordination. By providing a principled means of identifying redundant versus complementary features, ICrA has the potential to support balanced feature pre-selection in future machine-learning models aimed at improving early detection, differential diagnosis, and longitudinal monitoring of neurodegenerative disorders through gait.

Supplementary Materials: The following supporting information can be downloaded at https://www.mdpi.com/article/10.3390/math14020340/s1. The Supplementary Material S1 provides additional ICrA results for disease severity (Table S1) and gender (Table S2), introduces a normalized ICrA correlation framework, and benchmarks population-level intercriteria relationships against Pearson correlation analysis (Figures S1 and S2, Tables S3 snd S4).

Author Contributions: Conceptualization, I.J., V.K. and T.S.; methodology, I.J. and V.K.; software, I.J., V.K. and T.S.; validation, I.J. and V.K.; formal analysis, I.J. and V.K.; investigation, I.J., V.K. and T.S.; resources, I.J., V.K. and T.S.; data curation, I.J., V.K. and T.S.; writing—original draft preparation, I.J. and V.K.; writing—review and editing, I.J., V.K. and T.S.; visualization, I.J. and V.K.; project administration, I.J. and V.K.; funding acquisition, I.J. All authors have read and agreed to the published version of the manuscript.

Funding: This research was funded by Bulgarian National Science Fund, grant number КП-06-H77/13—"Studying locomotor and physiological activity using biocompatible and antibacterial multimodal sensors".

Institutional Review Board Statement: Not applicable.

Informed Consent Statement: Not applicable.

Data Availability Statement: The Gait in Neurodegenerative Disease Database is available at https://www.physionet.org/content/gaitndd/1.0.0/ (accessed on 6 January 2026). The implementation of the InterCriteria Analysis ICrAData v.2.3 is available at https://intercriteria.net/software/icradata/ (accessed on 6 January 2026).

Conflicts of Interest: The authors declare no conflicts of interest. The funders had no role in the design of the study; in the collection, analyses, or interpretation of data; in the writing of the manuscript; or in the decision to publish the results.

References

1. Ciurea, A.V.; Mohan, A.G.; Covache-Busuioc, R.-A.; Costin, H.-P.; Glavan, L.-A.; Corlatescu, A.-D.; Saceleanu, V.M. Unraveling Molecular and Genetic Insights into Neurodegenerative Diseases: Advances in Understanding Alzheimer's, Parkinson's, and Huntington's Diseases and Amyotrophic Lateral Sclerosis. *Int. J. Mol. Sci.* **2023**, *24*, 10809. [CrossRef]
2. Beyrami, S.M.G.; Ghaderyan, P. A robust, cost-effective and non-invasive computer-aided method for diagnosis three types of neurodegenerative diseases with gait signal analysis. *Measurement* **2020**, *156*, 107579. [CrossRef]
3. Dorsey, E.R.; Elbaz, A.; Nichols, E.; Abd-Allah, F.; Abdelalim, A.; Adsuar, J.C.; Ansha, M.G.; Brayne, C.; Choi, J.-Y.J.; Collado-Mateo, D. Global, Regional, and National Burden of Parkinson's Disease, 1990–2016: A Systematic Analysis for the Global Burden of Disease Study 2016. *Lancet Neurol.* **2018**, *17*, 939–953. [CrossRef]
4. Mathis, S.; Goizet, C.; Soulages, A.; Vallat, J.-M. Genetics of amyotrophic lateral sclerosis: A review. *J. Neurol. Sci.* **2019**, *15*, 217–226. [CrossRef]
5. Gadhave, D.G.; Sugandhi, V.V.; Jha, S.K.; Nangare, S.N.; Gupta, G.; Singh, S.K.; Dua, K.; Cho, H.; Hansbro, P.M.; Paudel, K.R. Neurodegenerative disorders: Mechanisms of degeneration and therapeutic approaches with their clinical relevance. *Ageing Res. Rev.* **2024**, *99*, 102357. [CrossRef]
6. Lamptey, R.N.L.; Chaulagain, B.; Trivedi, R.; Gothwal, A.; Layek, B.; Singh, J. A Review of the Common Neurodegenerative Disorders: Current Therapeutic Approaches and the Potential Role of Nanotherapeutics. *Int. J. Mol. Sci.* **2022**, *23*, 1851. [CrossRef]
7. Harmanşa, Y.K.; Erbaş, O. Diagnostic and Therapeutic Biomarkers for Neurodegeneration. *J. Exp. Basic Med. Sci.* **2022**, *3*, 47–53. [CrossRef]

8. Politis, M.; Wu, K.; Molloy, S.; Bain, P.G.; Chaudhuri, K.R.; Piccini, P. Parkinson's Disease Symptoms: The Patient's Perspective. *Mov. Disord.* **2010**, *25*, 1646–1651. [CrossRef] [PubMed]
9. Balestrino, R.; Schapira, A.H.V. Parkinson Disease. *Eur. J. Neurol.* **2020**, *27*, 27–42. [CrossRef] [PubMed]
10. Bhat, S.; Acharya, U.R.; Hagiwara, Y.; Dadmehr, N.; Adeli, H. Parkinson's Disease: Cause Factors, Measurable Indicators, and Early Diagnosis. *Comput. Biol. Med.* **2018**, *102*, 234–241. [CrossRef]
11. Carvalho, L.P.; Mate, K.K.V.; Cinar, E.; Abou-Sharkh, A.; Lafontaine, A.-L.; Mayo, N.E. A new approach toward gait training in patients with Parkinson's Disease. *Gait Posture* **2020**, *81*, 14–20. [CrossRef]
12. Moreau, C.; Cantiniaux, S.; Delval, A.; Defebvre, L.; Azulay, J.-P. Gait disorders in Parkinson's disease: And pathophysiological approaches. *Rev. Neurol.* **2010**, *166*, 158–167. [CrossRef]
13. Koller, W.C.; Trimble, J. The gait abnormality of Huntington's disease. *Neurology* **1985**, *35*, 1450–1454. [CrossRef] [PubMed]
14. Delval, A.; Krystkowiak, P.; Blatt, J.L.; Labyt, E.; Dujardin, K.; Destée, A.; Derambure, P.; Defebvre, L. Role of hypokinesia and bradykinesia in gait disturbances in Huntington's disease: A biomechanical study. *J. Neurol.* **2006**, *253*, 73–80. [CrossRef]
15. Dubbioso, R.; Spisto, M.; Hausdorff, J.M.; Aceto, G.; Iuzzolino, V.V.; Senerchia, G.; De Marco, S.; Marcuccio, L.; Femiano, C.; Iodice, R.; et al. Cognitive impairment is associated with gait variability and fall risk in amyotrophic lateral sclerosis. *Eur. J. Neurol.* **2023**, *30*, 3056–3067. [CrossRef] [PubMed]
16. Hausdorff, J.M.; Lertratanakul, A.; Cudkowicz, M.E.; Peterson, A.L.; Kaliton, D.; Goldberger, A.L. Dynamic markers of altered gait rhythm in amyotrophic lateral sclerosis. *J. Appl. Physiol.* **2000**, *88*, 2045–2053. [CrossRef] [PubMed]
17. Goldfarb, B.J.; Simon, S.R. Gait patterns in patients with amyotrophic lateral sclerosis. *Arch. Phys. Med. Rehabil.* **1984**, *65*, 61–65.
18. Berry, J.D.; Blanchard, M.; Bonar, K.; Drane, E.; Murton, M.; Ploug, U.; Ricchetti-Masterson, K.; Savic, N.; Worthington, E.; Heiman-Patterson, T. Epidemiology and economic burden of amyotrophic lateral sclerosis in the United States: A literature review. *Amyotroph. Lateral Scler. Front. Degener.* **2023**, *24*, 436–448. [CrossRef] [PubMed]
19. Kruse, C.; Lipinski, A.; Verheyen, M.; Balzer-Geldsetzer, M.; Wittenberg, M.; Lorenzl, S.; Richinger, C.; Schmotz, C.; Tönges, L.; Woitalla, D.; et al. Care of Late-Stage Parkinsonism: Resource Utilization of the Disease in Five European Countries. *Mov. Disord.* **2024**, *39*, 571–584. [CrossRef] [PubMed]
20. Rodríguez-Santana, I.; Mestre, T.; Squitieri, F.; Willock, R.; Arnesen, A.; Clarke, A.; D'Alessio, B.; Fisher, A.; Fuller, R.; Hamilton, J.L.; et al. Economic burden of Huntington disease in Europe and the USA: Results from the Huntington's Disease Burden of Illness study. *Eur. J. Neurol.* **2023**, *30*, 1109–1117. [CrossRef]
21. Achtert, K.; Kerkemeyer, L. The economic burden of amyotrophic lateral sclerosis: A systematic review. *Eur. J. Health Econ.* **2021**, *22*, 1151–1166. [CrossRef]
22. Beck, M.; Giess, R.; Würffel, W.; Magnus, T.; Ochs, G.; Toyka, K.V. Comparison of maximal voluntary isometric contraction and Drachman's hand-held dynamometry in evaluating patients with amyotrophic lateral sclerosis. *Muscle Nerve* **1999**, *22*, 1265–1270. [CrossRef]
23. Bowser, R.; Cudkowicz, M.; Kaddurah-Daouk, R. Biomarkers for amyotrophic lateral sclerosis. *Expert Rev. Mol. Diagn.* **2006**, *6*, 387–398. [CrossRef]
24. Erdaş, Ç.B.; Sümer, E.; Kibaroğlu, S. Neurodegenerative diseases detection and grading using gait dynamics. *Multimed. Tools Appl.* **2023**, *82*, 22925–22942. [CrossRef]
25. Khera, P.; Kumar, A.; Kapila, R. Decision tree for severity assessment of neurodegenerative diseases using possibility approach and gait dynamics. *Sci. Rep.* **2025**, *15*, 26247. [CrossRef] [PubMed]
26. Ru, Y.; Zhao, X.; Baghersad, Y.; Andani, H.T.; Hekmatifar, M.; Bouallegue, B. Gait analysis and Machine learning algorithms to distinguish between Parkinson's disease, amyotrophic lateral sclerosis, and Huntington's disease. *Biomed. Signal Process. Control* **2025**, *110*, 108216. [CrossRef]
27. Cicirelli, G.; Impedovo, D.; Dentamaro, V.; Marani, R.; Pirlo, G.; D'Orazio, T.R. Human Gait Analysis in Neurodegenerative Diseases: A Review. *IEEE J. Biomed. Health Inform.* **2022**, *26*, 229–242. [CrossRef]
28. Atanassov, K.; Mavrov, D.; Atanassova, V. Intercriteria Decision making: A new approach for multicriteria decision making, based on index matrices and intuitionistic fuzzy sets. *Issues IFSs GNs* **2014**, *11*, 1–8.
29. Atanassov, K.; Atanassova, V.; Gluhchev, G. Intercriteria analysis: Ideas and problems. *Notes Intuitionistic Fuzzy Sets* **2015**, *21*, 81–88.
30. Atanassova, V. Interpretation in the intuitionistic fuzzy triangle of the results, obtained by the intercriteria analysis. In *Proceedings of the 2015 Conference of the International Fuzzy Systems Association and the European Society for Fuzzy Logic and Technology (IFSA-EUSFLAT-15), Gijón, Spain, 30 June 2015*; Atlantis Press: Paris, France, 2015; pp. 1369–1374.
31. Doukovska, L.; Atanassova, V.; Sotirova, E.; Vardeva, I.; Radeva, I. Defining consonance thresholds in intercriteria analysis: An overview. *Stud. Comput. Intell.* **2019**, *757*, 161–179.
32. Pencheva, T.; Roeva, O.; Angelova, M. Investigation of genetic algorithm performance based on different algorithms for intercriteria relations calculation. *Lect. Notes Comput. Sci.* **2018**, *10665*, 390–398.

33. Vassilev, P.; Ribagin, S.; Todorova, L. On an aggregation of expert value assignments using index matrices. *Notes Intuitionistic Fuzzy Sets* **2017**, *23*, 75–78.
34. Roeva, O.; Pencheva, T.; Angelova, M.; Vassilev, P. Intercriteria analysis by pairs and triples of genetic algorithms application for models identification. *Stud. Comput. Intell.* **2016**, *655*, 193–218.
35. Traneva, V.; Tranev, S.; Kahraman, C. A multidimensional intuitionistic fuzzy InterCriteria analysis in the restaurant. *J. Intell. Fuzzy Syst. Appl. Eng. Technol.* **2020**, *39*, 6059–6071. [CrossRef]
36. Tsakovska, I.; Alov, P.; Ikonomov, N.; Atanassova, V.; Vassilev, P.; Roeva, O.; Jereva, D.; Atanassov, K.; Pajeva, I.; Pencheva, T. Intercriteria analysis implementation for exploration of the performance of various docking scoring functions. *Stud. Comput. Intell.* **2021**, *902*, 88–98.
37. Vankova, D.; Sotirova, E.; Bureva, V. An application of the intercriteria analysis approach to health-related quality of life. *Notes Intuitionistic Fuzzy Sets* **2015**, *21*, 40–48.
38. Todinova, S.; Mavrov, D.; Krumova, S.; Marinov, P.; Atanassova, V.; Atanassov, K.; Taneva, S.G. Blood plasma thermograms dataset analysis by means of intercriteria and correlation analyses for the case of colorectal cancer. *Int. J. Bioautomat.* **2016**, *20*, 115–124.
39. Krumova, S.; Todinova, S.; Mavrov, D.; Marinov, P.; Atanassova, V.; Atanassov, K.; Taneva, S. Intercriteria analysis of calorimetric data of blood serum proteome. *Biochim. Biophys. Acta Gen. Subj.* **2017**, *1861*, 409–417. [CrossRef]
40. Sotirov, S.; Petrova, Y.; Bozov, H.; Sotirova, E. A Hybrid Algorithm for Multilayer Perceptron Design with Intuitionistic Fuzzy Logic Using Malignant Melanoma Disease Data. In *Proceedings of the International Conference on Intelligent and Fuzzy Systems (INFUS 2022), Izmir, Turkey, 19–21 July 2022*; Kahraman, C., Tolga, A.C., Cevik Onar, S., Cebi, S., Oztaysi, B., Sari, I.U., Eds.; Springer: Berlin/Heidelberg, Germany, 2022; Volume 504. [CrossRef]
41. Zaharieva, B.; Doukovska, L.; Ribagin, S.; Radeva, I. Intercriteria analysis of data obtained from patients with Behterev's disease. *Int. J. Bioautomat.* **2020**, *24*, 5–14. [CrossRef]
42. Jekova, I.; Vassilev, P.; Stoyanov, T.; Pencheva, T. InterCriteria Analysis: Application for ECG Data Analysis. *Mathematics* **2021**, *9*, 854. [CrossRef]
43. Dobrev, P.; Sotirova, E. An Intelligent Data Analysis Approach for Women with Menopausal Genitourinary Syndrome with Intuitionistic Fuzzy Logic. In *Proceedings of the International Conference on Intelligent and Fuzzy Systems 2023 (INFUS 2023), Istanbul, Turkey, 22–24 August 2023*; Kahraman, C., Sari, I.U., Oztaysi, B., Cebi, S., Cevik Onar, S., Tolga, A.Ç., Eds.; Springer: Berlin/Heidelberg, Germany, 2023; Volume 758. [CrossRef]
44. Angelova, S.; Angelova, M.; Raikova, R. Estimating Surface EMG Activity of Human Upper Arm Muscles Using InterCriteria Analysis. *Math. Comput. Appl.* **2024**, *29*, 8. [CrossRef]
45. Angelova, M.; Angelova, S.; Raikova, R. How to Optimize the Experimental Protocol for Surface EMG Signal Measurements Using the InterCriteria Decision-Making Approach. *Appl. Sci.* **2024**, *14*, 5436. [CrossRef]
46. Mancheva, K.; Angelova, M.; Kossev, A.; Angelova, S. Assessing the Effects of TMS Intensities and Muscle Conditions on the Evoked Responses of the First Dorsal Interosseous Muscle Using Statistical Methods and InterCriteria Analysis. *Appl. Sci.* **2025**, *15*, 5236. [CrossRef]
47. Angelova, S.; Raikova, R.; Angelova, M. Intercriteria Decision-Making Method for Speed and Load Effects Evaluation on Upper Arm Muscles in the Horizontal Plane. *Appl. Sci.* **2025**, *15*, 11213. [CrossRef]
48. Goldberger, A.; Amaral, L.; Glass, L.; Hausdorff, J.; Ivanov, P.C.; Mark, R.; Mietus, J.E.; Moody, G.B.; Peng, C.-K.; Stanley, H.E. PhysioBank, PhysioToolkit, and PhysioNet: Components of a new research resource for complex physiologic signals. *Circulation* **2000**, *101*, e215–e220. [CrossRef] [PubMed]
49. Hausdorff, J. *Gait in Neurodegenerative Disease Database*; Version: 1.0.0; PhysioNet: Cambridge, MA, USA, 2000; Available online: https://www.physionet.org/content/gaitndd/1.0.0/ (accessed on 4 November 2025).
50. Murray, M.P.; Drought, A.B.; Kory, R.C. Walking patterns of normal men. *J. Bone Jt. Surg. Am.* **1974**, *56*, 777–790. [CrossRef]
51. Perry, J.; Burnfield, J.M. *Gait Analysis: Normal and Pathological Function*, 2nd ed.; SLACK Incorporated: Thorofare, NJ, USA, 2010.
52. Whittle, M.W. *Gait Analysis: An Introduction*, 5th ed.; Butterworth-Heinemann: Oxford, UK, 2014.
53. Erdaş, Ç.B.; Sümer, E. CNN-Based Neurodegenerative Disease Classification Using QR-Represented Gait Data. *Brain Behav.* **2024**, *14*, e70100. [CrossRef]
54. Yang, M.; Zheng, H.; Wang, H.; McClean, S. Feature Selection and Construction for the Discrimination of Neurodegenerative Diseases Based on Gait Analysis. In Proceedings of the 3rd International Conference on Pervasive Computing Technologies for Healthcare, London, UK, 1–3 April 2009; pp. 1–7. [CrossRef]
55. Xia, Y.; Gao, Q.; Ye, Q. Classification of Gait Rhythm Signals Between Patients with Neuro-degenerative Diseases and Normal Subjects: Experiments with Statistical Features and Different Classification Models. *Biomed. Signal Process. Control* **2015**, *18*, 254–262. [CrossRef]
56. Hausdorff, J.M. Gait variability: Methods, modeling and meaning. *J. NeuroEng. Rehabil.* **2005**, *2*, 19. [CrossRef] [PubMed]

57. Galna, B.; Lord, S.R.; Rochester, L. Is gait variability reliable in older adults and Parkinson's disease? Towards an optimal testing protocol. *Gait Posture* **2013**, *37*, 580–585. [CrossRef] [PubMed]
58. Lin, D.C.; McGowan, C.P.; Blum, K.P.; Ting, L.H. Yank: The Time Derivative of Force is an Important Biomechanical Variable in Sensorimotor Systems. *J. Exp. Biol.* **2019**, *222*, jeb180414. [CrossRef]
59. Andersen, L.L.; Aagaard, P. Influence of maximal muscle strength and intrinsic muscle contractile properties on contractile rate of force development. *Eur. J. Appl. Physiol.* **2006**, *96*, 46–52. [CrossRef]
60. Maffiuletti, N.A.; Aagaard, P.; Blazevich, A.J.; Folland, J.; Tillin, N.; Duchateau, J. Rate of force development: Physiological and methodological considerations. *Eur. J. Appl. Physiol.* **2016**, *116*, 1091–1116. [CrossRef] [PubMed]
61. Bohannon, R.W. Considerations and Practical Options for Measuring Muscle Strength: A Narrative Review. *BioMed Res. Int.* **2019**, *2019*, 8194537. [CrossRef]
62. Winter, D.A. *The Biomechanics and Motor Control of Human Gait: Normal, Elderly and Pathological*, 2nd ed.; University of Waterloo Press: Waterloo, ON, Canada, 1991.
63. Aagaard, P.; Simonsen, E.B.; Andersen, J.L.; Magnusson, P.; Dyhre-Poulsen, P. Increased rate of force development and neural drive of human skeletal muscle following resistance training. *J. Appl. Physiol.* **2002**, *93*, 1318–1326. [CrossRef] [PubMed]
64. Winter, D.A. *Biomechanics and Motor Control of Human Movement*, 4th ed.; John Wiley & Sons: Hoboken, NJ, USA, 2009.
65. Bendat, J.S.; Piersol, A.G. *Random Data: Analysis and Measurement Procedures*, 4th ed.; John Wiley & Sons: Hoboken, NJ, USA, 2010.
66. Robinson, R.O.; Herzog, W.; Nigg, B.M. Use of force platform variables to quantify the effects of chiropractic manipulation on gait symmetry. *J. Manip. Physiol. Ther.* **1987**, *10*, 172–176.
67. Herzog, W.; Nigg, B.M.; Read, L.J.; Olsson, E. Asymmetries in ground reaction force patterns in normal human gait. *Med. Sci. Sports Exerc.* **1989**, *21*, 110–114. [CrossRef]
68. Patterson, K.K.; Gage, W.H.; Brooks, D.; Black, S.E.; McIlroy, W.E. Evaluation of gait symmetry after stroke: A comparison of current methods and recommendations for standardization. *Gait Posture* **2010**, *31*, 241–246. [CrossRef]
69. Atanassov, K. Generalized index matrices. *Compt. Rend. Acad. Bulg. Sci.* **1987**, *40*, 15–18.
70. Atanassov, K. *Index Matrices: Towards an Augmented Matrix Calculus*; Springer: Cham, Switzerland, 2014.
71. Atanassov, K. Intuitionistic fuzzy sets. *Int. J. Bioautom.* **2016**, *20*, S1–S6.
72. Atanassov, K. *On Intuitionistic Fuzzy Sets Theory*; Springer: Cham, Switzerland, 2012.
73. Atanassov, K. *Intuitionistic Fuzzy Logics*; Springer: Cham, Switzerland, 2017.
74. Hošková-Mayerová, S.; Maturo, A. Decision-making process using hyperstructures and fuzzy structures in social sciences. *Stud. Fuzziness Soft Comput.* **2018**, *357*, 103–111. [CrossRef]
75. Szmidt, E.; Kacprzyk, J. An application of intuitionistic fuzzy set similarity measures to a multi-criteria decision making problem. *Lect. Notes Comput. Sci.* **2006**, *4029*, 314–323. [CrossRef]
76. Singh, A.P.; Athisayamani, S. Segmentation of Brain Tumors with Multi-kernel Fuzzy C-means Clustering in MRI. In *Data Engineering and Intelligent Computing*; Bhateja, V., Khin Wee, L., Lin, J.C.W., Satapathy, S.C., Rajesh, T.M., Eds.; Lecture Notes in Networks and Systems; Springer: Singapore, 2022; Volume 446. [CrossRef]
77. Atanassova, V.; Mavrov, D.; Doukovska, L.; Atanassov, K. Discussion on the Threshold Values in the InterCriteria Decision Making Approach. *Int. J. Notes Intuitionistic Fuzzy Sets* **2014**, *20*, 94–99.
78. Xie, C.; McCullum, L.; Johnson, A.; Pollard, T.; Gow, B.; Moody, B. Waveform Database Software Package (WFDB) for Python (version 4.1.0). In *PhysioNet*; RRID:SCR_007345; MIT Laboratory for Computational Physiology: Cambridge, MA, USA, 2023. [CrossRef]
79. Ikonomov, N.; Vassilev, P.; Roeva, O. ICrAData—Software for intercriteria analysis. *Int. J. Bioautom.* **2018**, *22*, 1–10. [CrossRef]
80. Keon, M.; Musrie, B.; Dinger, M.; Brennan, S.E.; Santos, J.; Saksena, N.K. Destination Amyotrophic Lateral Sclerosis. *Front. Neurol.* **2021**, *12*, 596006. [CrossRef]
81. Rushton, D.J.; Andres, P.L.; Allred, P.; Baloh, R.H.; Svendsen, C.N. Patients with ALS show highly correlated progression rates in left and right limb muscles. *Neurology* **2017**, *89*, 196–206. [CrossRef] [PubMed]
82. Nishikawa, Y.; Holobar, A.; Watanabe, K.; Takahashi, T.; Ueno, H.; Maeda, N.; Maruyama, H.; Tanaka, S.; Hyngstrom, A.S. Detecting Motor Unit Abnormalities in Amyotrophic Lateral Sclerosis Using High-density Surface EMG. *Clin. Neurophysiol.* **2022**, *142*, 262–272. [CrossRef]
83. Grimbergen, Y.A.M.; Knol, M.J.; Bloem, B.R.; Kremer, B.P.H.; Roos, R.A.C.; Munneke, M. Falls and gait disturbances in Huntington's disease. *Mov. Disord.* **2008**, *23*, 970–976. [CrossRef]
84. Talman, L.S.; Hiller, A.L. Approach to Posture and Gait in Huntington's Disease. *Front. Bioeng. Biotechnol.* **2021**, *9*, 668699. [CrossRef]
85. Morris, M.E.; Iansek, R.; Matyas, T.A.; Summers, J.J. Stride length regulation in Parkinson's disease. Normalization strategies and underlying mechanisms. *Brain* **1996**, *119*, 551–568. [CrossRef]

86. Giri, D.; Panigrahi, R.; Bhandari, S.S.; Pramanik, M.; de Albuquerque, V. Gait-Based Neurodegenerative Disease Detection via Recurrent Neural Networks. In *Proceedings of the Innovations in Data Analytics 2024 (ICIDA 2024), Kolkata, India, 18–19 December 2024*; Bhattacharya, A., Dutta, S., Yang, X.S., Goon, S., Eds.; Lecture Notes in Networks and Systems; Springer: Singapore, 2025; Volume 1408. [CrossRef]
87. Lin, C.-W.; Wen, T.-C.; Setiawan, F. Evaluation of Vertical Ground Reaction Forces Pattern Visualization in Neurodegenerative Diseases Identification Using Deep Learning and Recurrence Plot Image Feature Extraction. *Sensors* **2020**, *20*, 3857. [CrossRef]
88. Torghabeh, F.A.; Moghadam, E.A.; Hosseini, S.A. Simultaneous time-frequency analysis of gait signals of both legs in classifying neurodegenerative diseases. *Gait Posture* **2024**, *113*, 443–451. [CrossRef]
89. Rahman, K.A.; Shair, E.F.; Abdullah, A.R.; Lee, T.H.; Nazmi, N.; Zoha, M.S. Classifying Gait Disorder in Neurodegenerative Disorders Among Older Adults Using Deep Learning. In Proceedings of the 2024 IEEE-EMBS Conference on Biomedical Engineering and Sciences (IECBES), Penang, Malaysia, 11–13 December 2024; pp. 209–214. [CrossRef]
90. Setiawan, F.; Liu, A.-B.; Lin, C.-W. Development of Neuro-Degenerative Diseases' Gait Classification Algorithm Using Convolutional Neural Network and Wavelet Coherence Spectrogram of Gait Synchronization. *IEEE Access* **2022**, *10*, 38137–38153. [CrossRef]
91. Mengarelli, A.; Tigrini, A.; Fioretti, S.; Verdini, F. Identification of Neurodegenerative Diseases from Gait Rhythm Through Time Domain and Time-Dependent Spectral Descriptors. *IEEE J. Biomed. Health Inform.* **2022**, *26*, 5974–5982. [CrossRef] [PubMed]
92. Prabhu, P.; Karunakar, A.K.; Anitha, H.; Pradhan, N. Classification of gait signals into different neurodegenerative diseases using statistical analysis and recurrence quantification analysis. *Pattern Recognit. Lett.* **2020**, *139*, 10–16. [CrossRef]
93. Chatterjee, S. Analysis of the Human Gait Rhythm in Neurodegenerative Disease: A Multifractal Approach Using Multifractal Detrended Cross Correlation Analysis. *Phys. A Stat. Mech. Its Appl.* **2020**, *540*, 123154. [CrossRef]
94. Nguyen, Q.D.N.; Liu, A.-B.; Lin, C.-W. Development of a Neurodegenerative Disease Gait Classification Algorithm Using Multiscale Sample Entropy and Machine Learning Classifiers. *Entropy* **2020**, *22*, 1340. [CrossRef] [PubMed]

Disclaimer/Publisher's Note: The statements, opinions and data contained in all publications are solely those of the individual author(s) and contributor(s) and not of MDPI and/or the editor(s). MDPI and/or the editor(s) disclaim responsibility for any injury to people or property resulting from any ideas, methods, instructions or products referred to in the content.